The Characterization of the High-Frequency Vibronic Contributions to the 77 K Emission Spectra of Ruthenium−Am(m)ine−Bipyridyl Complexes, Their Attenuation with Decreasing Energy Gaps, and the Implications of Strong Electronic Coupling for Inverted-Region Electron Transfer

Puhui Xie, Yuan-Jang Chen, Md. Jamal Uddin, and John F. Endicott*

Department of Chemistry, Wayne State University, Detroit, Michigan 48202

Received: January 14, 2005; In Final Form: March 17, 2005

The 77 K emission spectra of a series of $[Ru(Am)_{6-2n}(bpy)_n]^{2+}$ complexes ($n = 1-3$) have been determined in order to evaluate the effects of appreciable excited state (e)/ground state (g) configurational mixing on the properties of simple electron-transfer systems. The principal focus is on the vibronic contributions, and the correlated distortions of the bipyridine ligand in the emitting MLCT excited state. To address the issues that are involved, the emission band shape at 77 K is interpreted as the sum of a fundamental component, corresponding to the $\{e,0'\} \rightarrow \{g,0\}$ transition, and progressions in the ground-state vibrational modes that correlate with the excited-state distortion. Literature values of the vibrational parameters determined from the resonance-Raman (rR) for $[Ru(NH_3)_4bpy]^{2+}$ and $[Ru(bpy)_3]^{2+}$ are used to model the emission spectra and to evaluate the spectral analysis. The Gaussian fundamental component with an energy E_f and bandwidth $\Delta\nu_{1/2}$ is deconvoluted from the observed emission spectrum. The first-, second-, and third-order terms in the progressions of the vibrational modes that contribute to the band shape are evaluated as the sums of Gaussian-shaped contributions of width $\Delta\nu_{1/2}$. The fundamental and the rR parameters give an excellent fit of the observed emission spectrum of $[Ru(NH_3)_4bpy]^{2+}$, but not as good for the $[Ru(bpy)_3]^{2+}$ emission spectrum probably because the Franck−Condon excited state probed by the rR is different in symmetry from the emitting MLCT excited state. Variations in vibronic contributions for the series of complexes are evaluated in terms of reorganizational energy profiles (emreps, Λ_x) derived from the observed spectra, and modeled using the rR parameters. This modeling demonstrates that most of the intensity of the vibronic envelopes obtained from the frozen solution emission spectra arises from the overlapping of first-order vibronic contributions of significant bandwidth with additional convoluted contributions of higher order vibronic terms. The emrep amplitudes of these complexes have their maxima at about 1500 cm^{-1} in frozen solution, and $\Lambda_{x(max)}$ decreases systematically by approximately 2-fold as E_f decreases from 17 220 for $[Ru(bpy)_3]^{2+}$ to 12 040 cm^{-1} for $[Ru(NH_3)_4bpy]^{2+}$ through the series of complexes. Corrections for higher order contributions and bandwidth differences based on the modeling with rR parameters indicate that the variations in $\Lambda_{x(max)}$ imply somewhat larger decreases in first-order bpy vibrational reorganizational energies. The large attenuation of vibrational reorganizational energies of the $[Ru(Am)_{6-2n}(bpy)_n]^{2+}$ complexes contrasts with the apparent similarity of reorganizational energy amplitudes for the absorption and emission of $[Ru(NH_3)_4bpy]^{2+}$. These observations are consistent with increasing and very substantial excited-state/ground-state configurational mixing and decreasing excited-state distortion as E_f decreases, but more severe attenuation for singlet/singlet than triplet/singlet mixing ($\alpha_{ge} > \alpha_{eg}$ for the configurational mixing coefficients at the ground-state and excited-state potential energy minima, respectively); it is inferred that $0.18 \geq \alpha_{ge}^2 \geq 0.09$ for $[Ru(bpy)_3]^{2+}$ and $0.37 \geq \alpha_{ge}^2 \geq 0.18$ for $[Ru(NH_3)_4bpy]^{2+}$ in DMSO/water glasses, where the ranges are based on models that there is or is not a spin restriction on configurational mixing ($\alpha_{ge} > \alpha_{eg}$ and $\alpha_{ge} = \alpha_{eg}$), respectively, for these complexes.

Introduction

Very strong donor−acceptor electronic coupling in an electron transfer system can result in alterations, relative to weak coupling limits, of the reaction driving force, the intrinsic barrier to reaction, and even the theoretical model used to describe the corresponding reaction rates. The complexes in which a metal acts as an electron donor (D) and a coordinated polypyridine ligand acts as an acceptor (A) typically have very intense metal-to-ligand charge transfer (MLCT) absorbencies, and this implies very strong D/A electronic coupling. Thus, electroabsorption measurements indicate that the electronic matrix element (H_{ge}; the subscripts denote ground, g, and excited, e, states) associated with the MLCT absorption for $[Ru^{II}(NH_3)_5py]^{2+}$ is about 10 000 cm^{-1},[1,2] and the comparison of a variety of measurements has suggested that $H_{ge} \approx 7000$ cm^{-1} for the corresponding transition in Ru^{II}−bipyridine complexes.[3] Consequently, the excited-state/ground-state transitions of these complexes should serve as good models for the investigation of the effects of strong electronic coupling on simple electron-transfer systems. Large electronic

* To whom correspondence should be addressed. E-mail: jfe@chem.wayne.edu.

10.1021/jp050263l CCC: $30.25
Published on Web 05/06/2005

matrix elements lead to appreciable configurational mixing between the corresponding diabatic electronic states.[4] For the mixing coefficient given by $\alpha_{ge} = H_{ge}/[E_{ge(d)}\{1 + (H_{ge}/E_{ge(d)})^2\}^{1/2}]$ (for $E_{ge(d)}$ the vertical energy difference between the two diabatic electronic states),[4] the mixing of electronic states should lead to systematic alterations in absorption and emission energies, bandwidths, and band shapes for a series of closely related complexes with a common chromophore but differences in E_{ge}. The bandwidths and band shapes are, in principle, functions of the contributions of the differences between the solvent and molecular nuclear coordinates, ΔQ_k, of the electronic ground and excited states.[5−16] Increases in configurational mixing between these states are expected to result in smaller differences in their nuclear coordinates. In a recent report,[17] we noted that the vibronic sidebands in the DACT emissions of a series of $[Ru(Am)_{6-2n}(bpy)_n]^{2+}$ complexes (Am = an am(m)ine) decrease systematically with the decreasing energy of the DACT emission, qualitatively consistent with the expected variations in the extent of configurational mixing. The present report addresses this attenuation of the vibronic sidebands of these complexes more systematically by means of an examination of the vibronic structure of their 77 K DACT emission spectra, and the comparison of these vibronic contributions to those expected based on previously reported resonance Raman (rR) spectra.[18,19]

This class of complexes has been very extensively studied,[20−28] but issues related to the extent and the effects of configurational mixing have been controversial,[21,27,29−33] and some issues that relate to the effects and variations of configurational mixing of the lowest energy MLCT excited state with other, near in energy electronic states are not well documented. For example, the high-energy MLCT excited states of $[Ru(bpy)_3]^{2+}$ have been found to cross between close-in-energy states of different formal spin multiplicities on subpicosecond time scales[34−37] and some of the electron injection into semiconductor substrates occurs on femtosecond time scales.[38,39] Since these electron transfer rates are faster than the rate of vibrational equilibration, they imply that Born−Oppernheimer approximation-based potential energy (PE) surfaces are not useful in describing them. It is not clear which molecular properties lead to these behaviors,[36] but the very large electronic matrix elements and the small energy differences between many of the electronic states[27] suggest that appreciable configurational mixing may play an important role.

The squared displacements, ΔQ_k^2, usually represented as vibrational reorganizational energies (λ_k) are important components of the Franck−Condon contributions to absorption and emission spectra,[12,13,40−44] to excited-state relaxation,[13,40,45,46] and to electron-transfer reactivity.[6,14,25,47−58] The absorption and emission spectra can be represented as sums of the contributions of progressions of vibrational contributions for each of the k displacements (whose vibrational frequencies = ν_k), and the λ_k contribute to the intrinsic bandwidths of the emission components for $h\nu_l < \sim 4k_BT$, and to the band shape for $h\nu_h > \sim 4k_BT$.[5−9,12,13,15,16,25,59−61] The evaluation of these reorganizational components is very often based on the properties of the separated donor and acceptor moieties. Thus, for very little configurational mixing and if other factors are not important the full width at half-height of each vibronic component of the emission is[62]

$$\Delta\nu_{1/2} \cong 4[k_BT\lambda_l \ln 2]^{1/2} \quad (1)$$

On the other hand, the observed band shape can be related to the contributions of higher frequency vibrational modes, and for small displacements the intensity of the first-order vibronic component of the hth displacement mode[10,11]

$$(I_{0'1})_h = (I_{0'0}/h\nu_h)\lambda_h \quad (2)$$

The variations in configurational mixing within a series of related complexes may result in different sets of values of the λ_k,[3,8,9,59,60] and one expects correlated variations in the experimentally observable spectroscopic properties. Thus, there should result variations in (1) absorption and emission zero point energies, (2) bandwidths, and (3) band shapes (or skewness). Standard perturbation theory arguments indicate that configurational mixing should alter zero point energies[4] and, more pertinent to the present report, very strongly affect the reorganizational energies.[3,8,9,60] Figure 1 qualitatively illustrates the effects of configurational mixing on the excited and ground-state PE surfaces; the changes in the PE surfaces result in changes in the emission band shapes. The effect on bandwidths is not as obvious since many factors contribute to the bandwidth of the observed emission envelope. It has been proposed that the bandwidths of the vibronic components (in the absence of other contributions) should be attenuated, compared to eq 1, with increasing configurational mixing[8,9,63] (for $\alpha_{eg} < 0.3$),

$$\Delta\nu_{1/2} \cong 4[k_BT\lambda_{l(d)}(1 - 4\alpha_{eg}^2) \ln 2]^{1/2} \quad (3)$$

In principle, eq 3 might be useful in establishing the variations in configurational mixing through a series of complexes. However, other factors can also contribute to the emission bandwidth. This is especially the case in solution studies since there is necessarily a distribution of solvation environments and this can alter bandwidths through the resulting range of values of $\lambda_{l(d)}$ and/or $E_{eg(d)}$. A perturbation theory treatment of the effects of the configurational mixing of the ground and excited states leads to an expression for the attenuation of the overall reorganizational energy, λ_r, for the parameters evaluated at the excited-state PE minimum when $\alpha_{eg} = \alpha_{ge}$ (i.e., for fluorescence; the effects of spin restrictions on the reorganizational parameters[60] result in $\alpha_{eg} < \alpha_{ge}$, and are treated in the Discussion section) and for $\alpha_{eg}^2 < 0.1$,[3,60]

$$\lambda_r \approx \lambda_{r(d)}(1 - 4\alpha_{eg}^2) \quad (4)$$

The intensities of the emission components corresponding to the high-frequency vibrational modes ($h\nu_h \geq 4k_BT$) should be free of the inhomogeneous broadening and other effects that complicate the interpretation of the bandwidths. If the attenuation is the same for all the distortion modes, then decreases in the low-energy sideband intensity of the emission spectrum can be used to evaluate the overall changes in contributions of vibrational reorganizational energies even in solution spectra in which the individual vibronic components are not resolved.

We have recently generated empirical reorganizational energy profiles (emreps) from D/A emission spectra in order to facilitate the search for vibronic contributions of very high-frequency vibrational modes.[16,64] In the present paper we examine the use of emreps as a tool for determining variations in λ_k. In this report we describe our studies of the attenuations of vibrational reorganizational energies of the bipyridine ligand inferred from the 77 K emission spectra of $[Ru(Am)_{6-2n}(bpy)_n]^{2+}$ complexes. We have selected these complexes as the substrates for this study because (a) their excited state properties have been so extensively characterized, (b) their very large MLCT absorptivities imply appreciable configurational mixing, (c) they exhibit a wide range of emission energies (Figure 2), (d) the vibrational modes of the bpy ligand have been noted to make distinct contributions to the band shape,[13,27] and (e) the emission in each complex, in

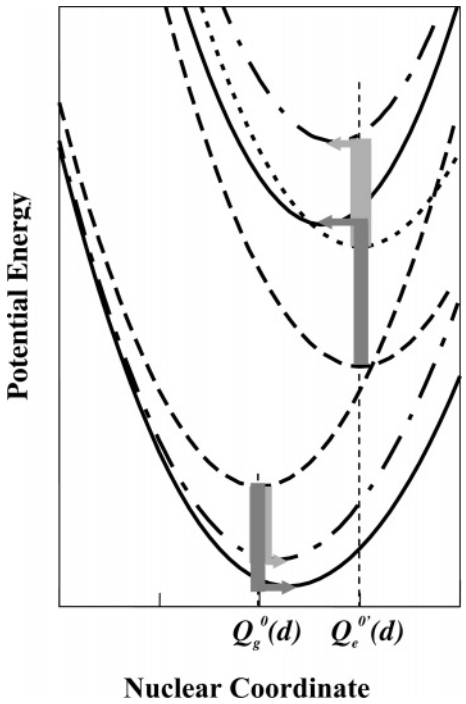

Figure 1. A qualitative comparison of the effects of configurational mixing on the ground state-excited state distortion in two closely related, very strongly coupled systems which differ only in their excited-state energies (upper dashed curves). The molecular distortion, $\Delta Q = Q_e^{0'} - Q_g^0$, decreases as the mixing increases; it is assumed that the electronic coupling matrix element, H_{ge}, is the same for the two systems and that the mixing coefficient, $H_{ge}/E_{ge}^{0'0}(d)$, depends only on the energy difference of the diabatic states, $E_{ge}^{0'0}(d)$. The dashed curves represent the (unmixed) diabatic states, the solid and dash-dot curves represent the adiabatic states (after mixing), and the arrows indicate the direction of shift of the respective PE minima (dark gray for the smallest $E_{ge}^{0'0}$, light gray for the largest.). Note that the actual distortion is between the adiabatic minima, block arrows.

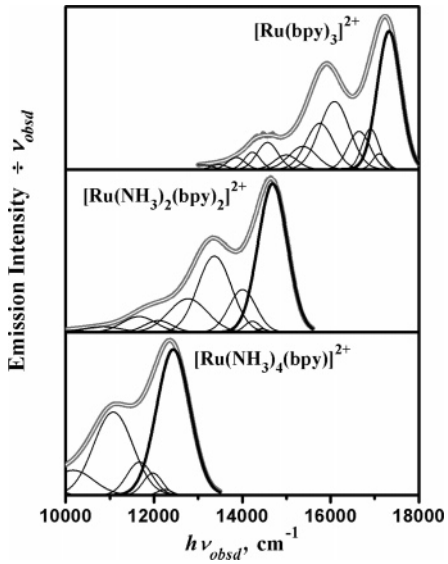

Figure 2. Comparison of the emission spectra and spectral deconvolutions for the $[Ru(NH_3)_{(6-2n)}(bpy)_n]^{2+}$ complexes. The black envelope line is the original spectrum and the superimposed whiter line is the fitted spectrum. The largest, high-energy Gaussian component (heavy black line) is assigned as the fundamental. Spectra were obtained at 77 K in butyronitrile glasses.

the simplest limit can be attributed to a common electronic transition: $\{bpy^-, Ru^{III}\} \rightarrow \{bpy, Ru^{II}\}$.

The vibronic contributions of the MLCT spectra of transition metal complexes in ambient solution are often difficult to determine: both absorption and emission spectra tend to have large bandwidths that obscure the contributions of individual components, and absorption spectra may be further complicated by the convolution of several electronic transitions into the absorption envelope.[3,59,60] Emission spectra in frozen solutions are more useful for the comparison of the excited states of a related series of complexes because the transitions almost always involve a single excited and a single ground electronic state, the contribution of the $\{e,0'\} \rightarrow \{g,0\}$ fundamental component of the emission is relatively easy to identify, some vibronic features can be resolved, and environmental differences between complexes can be minimized. The interpretation of the vibronic sidebands of even frozen solution emission specrtra is complicated by the substantial component bandwidths and the resulting convolution of the contributions when there are many contributing vibrational modes in the energy region examined.[31,32] We have used published resonance-Raman (rR) data reported for $[Ru(bpy)_3]^{2+}$ [19] and for $[Ru(NH_3)_4bpy]^{2+}$ [18] to examine the interpretation of the contributions of vibronic sidebands to the observed spectra.

Experimental Section

1. Materials. The ligands 2,2′-bipyridine (bpy) and ethylenediamine (en) were purchased from Aldrich and used without further purification. The complexes $[Ru(bpy)_3]Cl_2$, $RuCl_3 \cdot xH_2O$ ($x \leq 1$), *cis*-$Ru(bpy)_2Cl_2$, and $[Ru(NH_3)_5Cl]Cl_2$ were purchased from Strem Chemicals and used as received. The complexes $[Ru(NH_3)_5(O_3SCF_3)](O_3SCF_3)_2$,[65] $[Ru(NH_3)_4bpy](PF_6)_2$,[66−68] $[Ru(NH_3)_2(bpy)_2](PF_6)_2$,[66−68] $[Ru(bpy)]Cl_4$,[69] $[Ru(en)(bpy)_2](PF_6)_2$,[70] $[Ru(bpy)_2(O_3SCF_3)_2]$,[65] and $[Ru([14]aneN_4)bpy](PF_6)_2$[71] ([14]aneN$_4$ (cyclam) = 1,4,8,11-tetraazacyclotetradecane) were prepared by slight modifications of literature procedures (see the Supporting Information, S1).[72] All other reagents were reagent grade. Organic solvents were spectral grade, and water was deionized and distilled.

Elemental analyses of C, H, and N were performed at Midwest Micro Laboratories (Indianapolis, IN) and are summarized in Table S2a (Supporting Information).[72]

Am(m)ine deuterated complexes were prepared by dissolving the corresponding proteo-complex in D_2O and precipitating it by adding saturated $NaPF_6/D_2O$ solution into the mixture. This procedure was repeated several times and characterized either by IR spectra or by ^{1}H NMR. The ^{1}H NMR data are reported in Table S2b (Supporting Information).[72]

2. Instrumentation. Emission spectra at room temperature in the 500−800 nm range were recorded on a SPEX Fluorolog instrument, and corrected for instrument response with the correction file packaged with the instrument's software, or on a SPEX Tau-2 instrument in the 500−850 nm range with DataMax software. The Tau-2 detector response was useful to about 850 nm. Longer wavelength emission spectra and low-temperature emission spectra in 77 K glasses were determined with a Princeton Instruments (Roper Scientific) OMAV/InGaAS array detector mounted on an Acton SP500 spectrometer. The InGaAs detector response is relatively poor for wavelengths shorter than about 750 nm. For a few complexes with higher energy emissions, such as $[Ru(bpy)_3]^{2+}$, we have used the spectra determined using the InGaAs detector and second-order diffraction of the Acton spectrometer (in addition to the calibrated spectra determined with the SPEX Tau2). The intensity responses of the Tau2 and InGaAs-based spectrometers were calibrated with respect to the intensity output of an Oriel

Model 63358 Quartz Tungsten Halogen lamp with NIST traceable calibrated intensity output. The wavelength response of the InGaAs spectrometer was calibrated with respect to the Xe emission lines of an Oriel Spectral Calibration Lamp (model 6033). The emission data from the InGaAs spectrometer were collected using the WinSpec program. Emission measurements at 77 K were made using butyronitrile, DMSO:H_2O (1:1), or DMSO:D_2O (1:1) glasses or the microcrystalline solid in 1 mm i.d. cylindrical luminescence cells immersed in liquid nitrogen in a quartz Dewar secured with a Derlin holder. Microcrystalline solid samples were prepared by allowing solutions of the complexes to evaporate in the luminescence sample cells. The sample cell and Dewar were aligned for each experiment to optimize the signal. Optical filters were used to reduce the scattered laser light. At least 5−10 spectral scans were accumulated and averaged for each sample spectrum. Over the course of this study spectra were accumulated for several samples, and different preparations for each complex. We also compared the spectra obtained on two or more instruments for key compounds. We were able to obtain very good second-order emission spectra of $[Ru(bpy)_3]^{2+}$ (1100−1600 nm region) with the InGaAs detector-based system. Emission spectra obtained in the Tau2 and InGaAs-based spectrometers differed in their peak maxima by about 20 cm^{-1}. The Tau2 response to the Xe Spectral Calibration Lamp indicated a somewhat periodic deviation of about ±1 nm in wavelength responses.

Luminescence lifetimes were determined by passing the emitted light through an ISA H-100 monochromator to a Hammamatsu 950 PMT. The PMT was coupled to a LeCroy 9310 digital oscilloscope and interfaced to a computer.[10] Software for this system was written by OLIS, Inc. (Jefferson, GA).

The electrochemical measurements were performed with a BAS model 100A electrochemical workstation using manufacturer-supplied software for instrument control and data manipulation. Cyclic voltammograms (CV) were obtained using a three-electrode system consisting of a Ag/AgCl reference electrode, a Pt wire counter electrode, and a Pt disk working electrode for measurements in dry CH_3CN. The working electrode was polished with 0.3 and 0.05 μm Buehler alumina suspensions and sonicated for a few seconds between polishing cycles. The solutions consisted of the complex dissolved in acetonitrile containing 0.1 mol/L TBAH (tetrabutylammonium hexafluorophosphate) as electrolyte. Cyclic voltammograms were referenced internally to ferrocene (0.437 V vs Ag/AgCl) dissolved in the same sample solutions. The data are summarized in Table S3.[72]

UV−visible spectra were recorded using a Shimadzu UV-2101PC spectrophotometer. ^{1}H NMR spectra were performed using a Varian 300 Hz instrument.

3. Data Analysis Procedures. *a. Emission Spectra.* To evaluate the fundamental component, the spectrometer ASCII files were transferred to Excel and the observed spectral intensities were divided by the emission energy (see eq 6 below) and the intensity of the emission maximum was adjusted to 1.00. The resulting spectral data were transferred to Grams-32 for the Gaussian deconvolution. These fits were constructed so that the Gaussian function representing the fundamental, $I_{\nu_m(f)}$, matched the slope on the high-energy side of the experimental emission as closely as possible while accounting for most of the intensity of the high-energy feature, as described elsewhere.[3,64] These deconvolutions are based on the representation of the emission spectra as summations over Gaussian functions corresponding to the fundamental ($j = 0$) and other components.[12,14,43,44,73] Only the fundamental components obtained by this deconvolution procedure were used in the further analysis of the band shape. The data reported here are for spectra with reproducible band shapes and bandwidths, and they are the average of 4−12 individually determined spectra. The spectral deconvolutions are illustrated in Figure 2. The further interpretation of these spectra is based on the more detailed model for progressions in vibronic components with Gaussian band shapes as described below.

b. Empirical Reorganizational Energy Profiles (*emreps*). The reorganizational energy profiles are based on eq 2 (solved for λ_h) and constructed from the difference of the intensities of the observed emission spectrum and those of the fundamental component from the, $I_{\nu_m(spec)} - I_{\nu_m(f)}$ ($I_{\nu_m(spec)}$ is the intensity of the observed emission spectrum at the frequency ν_m), then multiplying the resulting difference spectrum by $h\nu_x/I_{max(f)}$, and plotting the product vs $h\nu_x$, as described elsewhere;[16,64] see the Supporting Information.[72] The energy axis in the emrep is given by,

$$h\nu_x = 2[h\nu_{max(f)} - h\nu_m] - [\{h\nu_{max(f)} - h\nu_m\}^2 + (\Delta\nu_{1/2})^2/4 \ln 2]^{1/2} \quad (5)$$

in which $h\nu_d = [h\nu_{max(f)} - h\nu_m]$ is approximately corrected for the displacement of the maxima of the reorganizational energy components to higher energies than the corresponding maxima for the vibronic contributions to the emission spectrum when the vibronic components have significant bandwidths.[72]

4. Modeling the Emission Spectra of $[Ru(bpy)_3]^{2+}$ and $[Ru(NH_3)_4bpy]^{2+}$ Based on Vibrational Parameters from Resonance-Raman Spectra. Observed ambient and frozen solution spectra clearly contain information about the contributions of distortion modes, but the interpretation of these contributions is complicated by the appreciable bandwidths of the spectral components. Very low temperature, crystalline solid-state spectroscopic studies of $[Ru(bpy)_3]^{2+}$ [27] and ambient resonance-Raman (rR) spectra of $[Ru(bpy)_3]^{2+}$ [19] and $[Ru(NH_3)_4bpy]^{2+}$ [18] solutions have demonstrated that there are a large number of molecular distortion modes in these complexes; see Table 2. We have used the rR data to model the observed emission spectra of these two complexes. This allows us to examine some issues in regard to (a) the relevance of the rR data (obtained from the region of the MLCT absorption) to the emission (presumably from the triplet MLCT excited state), (b) the effects of bandwidth variations on the information that may be inferred from solution spectra about the basic molecular parameters (zero point energies, vibronic contributions, etc.), and (c) the extent to which emreps may be used to evaluate variations in high-frequency vibrational reorganizational energy contributions. We have used the rR parameters to evaluate most aspects of our spectral analysis.

a. A Gaussian Component Model of the Contributions of the Intensity Contributions of Vibronic Progressions. The emission intensity at a frequency ν_m can be represented in general form as,[12,42−44]

$$I_{\nu_m} = \frac{64\pi^4}{3h^3c^3 \ln 10} \frac{\nu_m \eta^3 H_{eg}^2 (\Delta\mu_{eg})^2}{(4\pi\chi_s k_B T)^{1/2}} (FC) \quad (6)$$

In eq 6, η is the index of refraction, c is the speed of light, H_{eg} is the electronic matrix element, and $H_{eg}\Delta\mu_{eg}/h\nu_m$ has been substituted for the transition dipole, M_{eg}.[12,42,74] Based on Gaussian band shapes and a wave packet model and for the contributions of a single vibrational mode, (FC) can be

TABLE 1: Spectroscopic Properties and Excited State Decay Rate Constants for $[Ru(Am)_{6-2n}(bpy)_n]^{2+}$ Complexes[a]

Ru^{II} complex [ligands]	$h\nu_{abs(max)}$	$h\nu_{em(max)}$, 298 K	$h\nu_{em(max)}$, 77 K	$h\nu_{max(f)}$, $[\Delta\nu_{1/2}]$, 77 K {$h\nu_{max(f)}$, $[\Delta\nu_{1/2}]$, 298 K}	$\Lambda_x(\nu_x)$, 77 K	k_{nr} (μs^{-1}), 77 K {k_{nr} (μs^{-1}), 298 K}
$[(bpy)_3]$	21.9 (d/w)	15.98 (d/w)	17.12 (d/w)	17.22 [0.68] (d/w) {16.53 [1.64] (d/w)}	1.16 (1.49) (d/w)	0.23 (d/w) {1.1 (d/w)}
		16.24 (bun)	17.25 (bun)	17.31 [0.64] (bun)	1.05 (1.50) (bun)	
$[(en)(bpy)_2]$	20.2 (d/w)	13.97 (d/w)	15.00 (d/w)	15.06 [0.78] (d/w)	1.00 (1.50) (d/w)	1.3 (d/w) {12.3 (d/w)}
	20.4 (bun)	14.35 (bun)	15.11 (bun)	15.16 [0.72] (bun)	0.88 (1.49) (bun)	0.69 (bun) {10.2 (bun)}
$[(NH_3)_2(bpy)_2]$	20.4 (d/w)	13.52 (d/w)	14.56 (d/w)	14.64 [0.91] (d/w)	0.99 (1.53) (d/w)	2.9 (d/w) {25 (d/w)}
	20.2 (bun)	13.98 (bun)	14.67 (bun)	14.70 [0.78] (bun)	0.86 (1.49) (bun)	1.7 (bun) {14.5 (bun)}
$[([14]aneN_4)(bpy)]$	19.0 (d/w)	12.94 (d/w)	13.96 (d/w)	14.01 [0.95] (d/w)	0.85 (1.44) (d/w)	1.59 (d/w) {22.8 (d/w)}
	19.3 (d/w)	13.38 (bun)	13.99 (bun)	14.03 [0.89] (bun)	0.81 (1.45) (bun)	0.975 (bun) {19.0 (bun)}
$[(en)_2(bpy)]$	19.1 (d/w)	11.81 (d/w)	12.82 (d/w)	12.88 [1.03] (d/w)	0.85 (1.45) (d/w)	26 (d/w)
	19.2 (bun)	12.59 (bun)	13.01 (bun)	13.05 [0.89] (bun)	0.78 (1.45) (bun)	9.5 (bun)
$[(NH_3)_4(bpy)]$	18.8 (d/w)		12.02 (d/w)	12.09 [1.11] (d/w)	0.81 (1.45) (d/w)	39 (d/w)
	19.0 (bun)		12.37 (bun)	12.42 [0.92] (bun)	0.80 (1.48) (bun)	22 (bun)
$[(d_4\text{-en})(bpy)_2]$	20.3 (d/w)[b]	14.0 (d/w)[b]	15.00 (d/w)[b]	15.08 [0.78] (d/w)	0.99 (1.51) (d/w)	0.66 (d/w)[b] {6.2 (d/w)[b]}
	20.4 (bun)[c]	14.5 (bun)[c]	15.0 (bun)[c]	15.17 [0.76] (bun)	0.77 (1.47) (bun)	0.41 (bun)[c] {9.0 (bun)[c]}
$[(ND_3)_2(bpy)_2]$	20.3 (d/w)[b]	13.7 (d/w)[b]	14.57 (d/w)[b]	14.66 [0.91] (d/w)	0.98 (1.55) (d/w)	1.3 (d/w)[b] {13.7 (d/w)[b]}
	20.3 (bun)[c]	14.1 (bun)[c]	14.5 (bun)[c]	14.62 [0.86] (bun)	1.01 (1.49) (bun)[c]	1.1 (bun)[c] {13 (bun)[c]}
$[(d_4\text{-}[14]aneN_4)(bpy)]$	19.0 (d/w)	12.94 (d/w)	13.94 (d/w)[b]	13.99 [0.97] (d/w)	0.85 (1.44) (d/w)	1.27 (d/w)[b] {19.0 (d/w)[b]}
$[(d_4\text{-en})_2(bpy)]$	19.0 (d/w)[b]		12.83 (d/w)[b]	12.89 [1.04] (d/w)	0.84 (1.47) (d/w)	8.4 (d/w)[b]
	19.2 (bun)[c]		12.9 (bun)[c]	12.98 [0.84] (bun)	0.82 (1.38) (bun)	5.1 (bun)[c] {41 (bun)[c]}
$[(ND_3)_4(bpy)]$	18.9 (d/w)[b]		12.04 (d/w)[b]	12.10 [1.13] (d/w)	0.80 (1.46) (d/w)	13 (d/w)[b]
	19.2 (bun)[c]		12.2 (bun)[c]	12.41 [0.93] (bun)	0.79 (1.51) (bun)	12 (bun)[c]

[a] All energies in units of $cm^{-1}/10^3$. Abbreviations: d/w = DMSO/water; bun = butyronitrile. [b] $DMSO/D_2O$. [c] Trace amounts of H_2O may have been present.

TABLE 2: Summary of Resonance-Raman Parameters

	for $[Ru(bpy)_3]^{2+}$[19]				for $[Ru(NH_3)_4bpy]^{2+}$[18]				
vibration (i)[a]	ν_i(K), cm^{-1}	Δ_i(K)	λ_i(K), cm^{-1}	S_i(K)	ν_i(H), cm^{-1}	Δ_i(H)	λ_i(H), cm^{-1}	S_i(H)	S_i(K)/S_i(H)[b]
5	1608	0.31	77	0.048	1605	0.38	116	0.072	0.68
6	1563	0.47	171	0.110	1548	0.36	101	0.065	1.69
7	1491	0.73	397	0.266	1481	0.55	224	0.151	1.76
8	1450	0		0					
9	1320	0.56	207	0.157	1331	0.41	111	0.084	1.87
10	1276	0.36	83	0.065					
11	1264	0.09	5	0.004	1260	0.15	14	0.011	0.36
12	1176	0.48	135	0.115	1172	0.30	53	0.045	2.55
13	1110	0.16	14	0.013					
14	1067	0.10	5	0.005					
15	1043	0.16	13	0.013	1027	0.32	52	0.051	0.25
16	766	0.14	8	0.010					
17	668	0.75	188	0.281	667	0.62	128	0.192	1.46
					456	0.27	17	0.036	
18	370	0.44	37	0.10	376	0.81	123	0.328	0.306
19	283	0.50	35	0.125	248	0.46	26	0.106	1.18

[a] Notation from Maruszewski et al.[19] [b] Ratio of relative, first-order vibronic intensities.

represented by,[12,43,44]

$$(\mathrm{FC}) = \sum_j F_{j,h}[e^{-\{4G_j^2 \ln 2/\Delta\nu_{1/2}^2\}}] \tag{7}$$

$$F_{j,h} = \frac{S_h^{\,j} e^{-S_h}}{j!}; \qquad S_h = \lambda_h/h\nu_h \tag{8}$$

$$G_j = E^{0'0} - \lambda_s - jh\nu_h - h\nu_m \tag{9}$$

The zero-point energy difference between the ground-state and excited-state PE surfaces, $E^{0'0}$, and the solvent reorganizational energy associated with the redistribution of charge, λ_s, are difficult to determine independently from the emission spectra of species in solution, so we have chosen to express the functions that are used in the evaluation of the emission spectra in terms of parameters that are experimentally accessible: (i) the full width at half-height, $\Delta\nu_{1/2}$, in the denominator of the exponential, in place of the more commonly used, solvent reorganizational free energy (χ_s); and (ii) the energy of the maximum of the fundamental component of the emission spectrum, $h\nu_{max(f)} = E^{0'0} - \lambda_s$. The maximum of the fundamental emission component can be related to thermodynamic and kinetic properties of the substrate,[6,14,47,48,73,75]

$$h\nu_{max(f)} = |\Delta G_{eg}^{\,o}| - \chi_s = E^{0'0} - \lambda_s \tag{10}$$

In eq 10, $\Delta G_{eg}^{\,o}$ is the standard free energy difference and between the zeroth vibrational levels of the excited-state and ground-state PE surfaces, and χ_s is the difference in the free energy of solvation for the ground state with the solvent configured as appropriate for the excited-state PE minimum and for the PE minimum of the ground state. These free energy quantities are often available from other kinds of measurements, e.g., estimates of their values are often based on electron-transfer kinetic data and on electrochemical measurements, respectively.[14,23,73,75]

In this model of the emission spectra we assume that all the distortion modes have significant rR intensities and that there are no differences in selection rules for rR contributions and vibronic contributions to the emission spectra. In constructing the higher order contributions to the emission spectra, we have

assumed that the harmonic and combination band contributions are weighted equally. In effect, this model assumes very low symmetry (see the following discussion of the spectral fits).

We have constructed the intensity of the $\{e,0'\} \rightarrow \{g,0\}$ transition (the fundamental; for $j = 0$) as a Gaussian function with maximum intensity $I_{max(f)}$ at a frequency of $\nu_{max(f)}$ and full width at half-height of $\Delta\nu_{1/2}$. The intensity of the fundamental at a frequency ν_m is,

$$I_{\nu_m(f)} \cong I_{max(f)} e^{-\{[h\nu_{max(f)} - h\nu_m]^2/(\Delta\nu_{1/2}^2/4 \ln 2)\}} \quad (11)$$

The first-order vibronic terms are constructed as:

$$I_{\nu_m(0'1)} \cong I_{max(f)} \sum_h \left(\frac{\lambda_h}{h\nu_h}\right) e^{-\{[h\nu_{max(f)} - h\nu_h - h\nu_m]^2/(\Delta\nu_{1/2}^2/4 \ln 2)\}} \quad (12)$$

The second-order vibronic terms are constructed as:

$$I_{\nu_m(0'2)} \cong \frac{I_{max(f)}}{2} \sum_i \sum_j \left(\frac{\lambda_i}{h\nu_i}\right)\left(\frac{\lambda_j}{h\nu_j}\right) e^{-\{[h\nu_{max(f)} - h\nu_i - h\nu_j - h\nu_m]^2/(\Delta\nu_{1/2}^2/4 \ln 2)\}} \quad (13)$$

The third-order terms are constructed as:

$$I_{\nu_m(0'3)} \cong \frac{I_{max(f)}}{6} \sum_i \sum_j \sum_k \times \left(\frac{\lambda_i}{h\nu_i}\right)\left(\frac{\lambda_j}{h\nu_j}\right)\left(\frac{\lambda_k}{h\nu_k}\right) e^{-\{[h\nu_{max(f)} - h\nu_i - h\nu_j - h\nu_k - h\nu_m]^2/(\Delta\nu_{1/2}^2/4 \ln 2)\}} \quad (14)$$

Then the intensity at a frequency ν_m is calculated as:

$$I_{\nu_m(calcd)} \cong I_{\nu_m(f)} + I_{\nu_m(0'1)} + I_{\nu_m(0'2)} + I_{\nu_m(0'3)} + \ldots \quad (15)$$

The graphical presentation of $I_{\nu_m(calcd)}$ vs ν_m is the theoretical spectrum constructed from resonance-Raman data. Note that $I_{max(f)}$ is a constant for any specific spectrum, but we do not relate the values of this parameter found for one complex to those found for another. The experimental spectrum is designated $I_{\nu_m(spec)}$.

The intensity of the fundamental is fixed relative to the intensities of the rR components, eq 2, but the intensity of the fundamental obtained from Gaussian deconvolution of the observed spectra, when combined with the rR components results in a spectrum that is 10−30% more intense than that observed. To fit the spectrum, the numerical file containing the fundamental and the rR-based components was either scaled in EXCEL to match the experimental spectrum at the emission maximum or transferred to Grams32 and the intensities were matched with those of the experimental spectrum by adjusting $I_{max(f)}$. The rR fits were further optimized by slightly altering $\Delta\nu_{1/2}$.

Results

1. The Observed Emission Spectra. The pertinent absorption, emission, and lifetime data are summarized in Table 1. The fittings of the fundamental to the observed emission spectra are illustrated for butyronitrile solutions in Figure 2. The MLCT excited state emissions of the am(m)ine−polypyridyl complexes are weak, even at 77 K, and at appreciably lower energies than that of the $[Ru(bpy)_3]^{2+}$ complex.

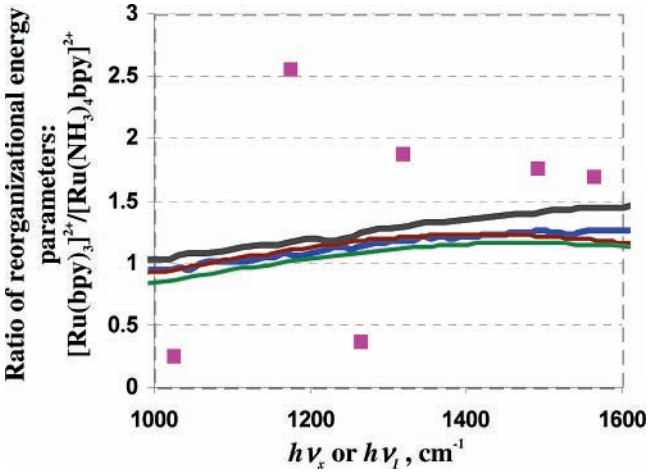

Figure 3. Ratio of reorganizational energy parameters in the range of bpy skeletal vibrations. Square points for reported rR components; ratio of Λ_x from experimental emission spectra in butyronitrile, heavy blue line; ratio of Λ_x from experimental emission spectra in DMSO/water, heavy black line; ratio of Λ_x based on emission spectra constructed from the reported rR parameters with the bandwidth observed in butyronitrile, brown line; ratio of Λ_x based on emission spectra constructed from the reported rR parameters with the bandwidth observed in DMSO/water, green line.

2. Observations on the Resonance-Raman Spectral Parameters Reported for $[Ru(bpy)_3]^{2+}$ and $[Ru(NH_3)_4bpy]^{2+}$. If the MLCT absorption in each complex corresponds to a $\{Ru^{II},bpy\} \rightarrow \{Ru^{III},bpy^-\}$ transition, then in the simplest limit one expects that the same bpy-centered vibrational modes contribute to both spectra. Equations 2 and 4, based on a two-state model, suggest that the ratio of the intensities of the first-order vibronic sidebands that originate from these vibrational modes of the two complexes is a constant that can be correlated to the electron density delocalized (α_{eg}^2). The relative intensities of the first-order vibrational mode contributions (S_i) obtained from the rR data of $[Ru(bpy)_3]^{2+}$ [19] and $[Ru(NH_3)_4bpy]^{2+}$ [18] are summarized in Table 2 and the ratios of these intensities in Figure 3. The ratios of these intensities for the two complexes vary over a considerable range: the apparent displacements in several modes are larger for $[Ru(bpy)_3]^{2+}$ than for $[Ru(NH_3)_4bpy]^{2+}$, as expected, but reversed for some of the other vibrational modes (Table 2 and Figure 3). The variations of the intensity ratios for the same vibrational modes in the different complexes has been noted previously.[43] A very similar pattern of variations of the relative intensities of the vibronic components has been observed for the rR spectra obtained from excitations of the MLCT absorption bands of $[Os(py)_{6-2n}(bpy)_n]^{2+}$ complexes.[76] Some differences are expected for $\nu_i < 1000$ cm^{-1} owing to differences in the metal−ligand skeletal vibrations, and there may also be some contributions in this range from the approach used to determine the displacements from the observed spectra.[18] Errors in the estimation of the low-frequency displacements will result in some smaller errors in the estimates of second-order terms. The variations of the relative intensities of the higher frequency vibronic terms must have a different origin. The resonance-Raman spectrum probes the Franck−Condon excited state,[43] and according to the Franck−Condon principle, this excited state and the ground state must have the same nuclear coordinates and symmetry. This corresponds to D_3 and C_{2v} symmetry for $[Ru(bpy)_3]^{2+}$ and $[Ru(NH_3)_4bpy]^{2+}$, respectively. This difference in symmetry necessarily corresponds to differences in the Franck−Condon excited state nuclear and electronic structure and this is likely to be the origin of the different apparent displacements in the bpy vibrational

modes. In fluid solution the excited state of $[Ru(bpy)_3]^{2+}$ apparently relaxes from the higher symmetry ("at least C_3'')[36] to the localized C_{2v} state in about 60 fs.[36] If this relaxation also occurs in frozen solution, then the rR data for $[Ru(bpy)_3]^{2+}$ do not properly describe the distortion of the emitting state.

Figure 3 compares (a) the ratios of the emreps based on the observed emission spectra of these complexes, (b) the ratios of the reorganizational energies of the reported rR frequencies,[18,19] and (c) the ratio of emreps based on the spectra calculated from the reported rR vibrational reorganizational energies and the bandwidth of the fundamental inferred from the observed emission spectra. If we discount the weakest rR vibrational modes (those with $\lambda_i < 10$ cm^{-1} for $[Ru(bpy)_3]^{2+}$), then the vibrations at about 1043 (1027) and 1608 (1605) cm^{-1} (reported vibrational frequencies of $[Ru(NH_3)_4bpy]^{2+}$ in parentheses) have smaller reorganizational energies for $[Ru(bpy)_3]^{2+}$ than for $[Ru(NH_3)_4bpy]^{2+}$, and the ratio of reorganizational energies for the 1176 (1172) vibrational mode seems anomalously large; this could also be the origin of the very large ratio of second-order contributions in the 2000−2400 cm^{-1} spectral region for the $[Ru(bpy)_3]^{2+}$ and $[Ru(NH_3)_4bpy]^{2+}$ emreps based on the spectral fits of the rR data ($\Delta\nu_{1/2} = 750$ and 1040 cm^{-1}, respectively, for both the fitted and experimental spectra).

Overall, the comparison of the rR data for the two complexes implies that the distortions of the bipyridyl ligands are different in their pattern as well as in amplitude for the two complexes. Likely origins of this effect are (a) differences in symmetry between the Franck−Condon excited state and the emitting state and/or (b) differences in the electronic states that are configurationally mixed with the emitting state. The Franck−Condon excited state of $[Ru(bpy)_3]^{2+}$ can be described as a symmetry adapted combination of the three equivalent diabatic MLCT excited states that each localize the excited electron on a different bpy ligand. This D_3, "delocalized" structure of the Franck−Condon excited state of $[Ru(bpy)_3]^{2+}$ and the C_{2v}, "localized" Franck−Condon excited state of $[Ru(NH_3)_4bpy]^{2+}$ should be expected to have different distortions. It is important to observe that a "delocalized" Franck−Condon excited state of $[Ru(bpy)_3]^{2+}$ need not have the same electron density in each of the bpy ligands since lowest energy MLCT excited states of $[Ru(bpy)_3]^{2+}$ are expected to have the $\{d\pi(e)^3,\pi^*(e)\}$, $\{d\pi(a_2),\pi^*(e)\}$ and $\{d\pi(e)^3,\pi^*(a_2)\}$ electronic configurations (where the Ru dπ-donor orbitals and the π^*-acceptor orbitals of the bpy ligands are adapted to D_3 symmetry). The MLCT excited states corresponding to the $\{d\pi(e)^3,\pi^*(e)\}$ configuration have ($A_1 + A_2 + E$) symmetries[77] and the $A_1 \rightarrow A_2$ and $A_1 \rightarrow E$ MLCT transitions are dipole allowed (z and x,y, respectively). The Franck−Condon excited states based on the $\{d\pi(e)^3,\pi^*(e)\}$ configuration will not have electron density equally distributed over the bpy ligands.

Even if the emitting ^{3}MLCT excited state of $[Ru(bpy)_3]^{2+}$ has the electron predominately localized in the π^* orbital of a single bpy, the vertical energy differences with the ^{3}MLCT′ excited states that "localize" the electron on the other two bpy ligands are small and there should be appreciable mixing of these excited states. This MLCT/MLCT′ configurational mixing is not available for $[Ru(NH_3)_4bpy]^{2+}$, and this difference in excited-state configurational mixing could result in excited-state distortions that are different in kind as well as degree. Some issues of the differences in distortion are illustrated by considering the subset of metal−ligand vibrational modes for the $[Ru(bpy)_3]^{2+}$ complex: in the C_2 limit (electron localized on a single bpy) there are 15 nondegenerate skeletal vibrations, while in the D_3 symmetry of the ground state there will only be 11 nondegenerate vibrations. This will result in differences in vibrational frequencies and probably differences in the relative displacements in the different modes. The skeletal modes of the bpy ligands are more complicated since there are three times as many vibrational modes in D_3 symmetry as in C_2 symmetry, and the vibrational modes of the individual bpy ligands must be properly adapted to D_3 symmetry. For example, there is a single breathing mode vibration (a symmetrical mode, a_s) in C_2 symmetry, and in the limit of weak configurational mixing the a_s modes of the three equivalent bpy ligands may be combined to construct two correlated vibrations (e and a_1) in D_3 symmetry. Even in this approximation the e vibrational mode is a weighted combination of the ligand a_s atomic motions of the individual ligands (e.g., $[2a_s - a_s' - a_s'']$ and $[a_s' - a_s'']$) and the correlated excited state displacements are not easily interpreted in terms of a single breathing motion. This linear combination of the ligand vibrational modes will be less useful when the configurational mixing is very strong, and it will be necessary to treat the coupled motions of the individual atoms of the ligands using some form of a normal coordinate analysis.

3. Fits of the Emission Spectra with the rR-Based Models. *a. The 77 K Spectra.* The rR-based models fit the 77 K emission spectra of both complexes quite well; however, the fit of the rR observations to the $[Ru(NH_3)_4bpy]^{2+}$ spectrum in Figure 4 is excellent while the fit is not as good for $[Ru(bpy)_3]^{2+}$. We have found that the fit of the vibrational parameters to the experimental emission spectrum of the latter is improved if the λ_i (or S_i) of $[Ru(bpy)_3]^{2+}$ are adjusted to equal 1.3−1.5 times the corresponding vibrational parameters for $[Ru(NH_3)_4bpy]^{2+}$ (Figure 4), but these fits are still not nearly as good as the fit of rR parameters to the $[Ru(NH_3)_4bpy]^{2+}$ emission.

Since the fundamentals make dominant contributions to both emission spectra and since we obtain a statistical best fit of the fundamental in these spectra, the quality of the fits of the rR data is most critically tested in the calculated difference spectra,

$$I_{\nu_m(\text{calcd,diff})} \cong I_{\nu_m(0'1)} + I_{\nu_m(0'2)} + I_{\nu_m(0'3)} + \ldots \qquad (16)$$

The difference spectrum calculated for $[Ru(NH_3)_4(bpy)]^{2+}$ from the rR data using eq 16 and obtained by subtracting the fundamental $I_{\nu_m(\text{exp;diff})} = (I_{\nu_m(\text{spec})} - I_f)$, where I_f is based on the Grams32 deconvolution and adjusted to be compatible with the rR vibronic components (see discussion below) from the observed spectrum are almost identical in shape and differ only slightly in amplitude (Figure 5). The 5−10% larger amplitude of the calculated difference spectrum is probably within the range of the uncertainties in our determinations of energies, intensities, and bandwidths that result from limitations of the optical alignment of the sample cell and the resolution and calibration of the detection system (see also Appendix A). However, this difference could also arise because the electronic state populated by absorption and probed by the rR is not the emitting state.[41,43]

There are much larger discrepancies of the calculated ($I_{\nu_m(\text{calcd;diff})}$) and observed ($I_{\nu_m(\text{exp;diff})}$) difference spectra for $[Ru(bpy)_3]^{2+}$, even when the ratios of vibronic intensities are fixed relative to those for $[Ru(NH_3)_4bpy]^{2+}$. Despite these discrepancies, it is important to note that the rR data do reasonably reproduce to the energies and amplitudes of the dominant features of the difference spectrum of $[Ru(bpy)_3]^{2+}$, and that the agreement is much better at high frequencies ($\nu_d > 1000$ cm^{-1}) than at low frequencies (see comments in section 2 above). This is also the case when the fundamental used to obtain the observed difference spectrum is based on the Grams32 deconvolution (not adjusted for the rR data, compare Figures 5

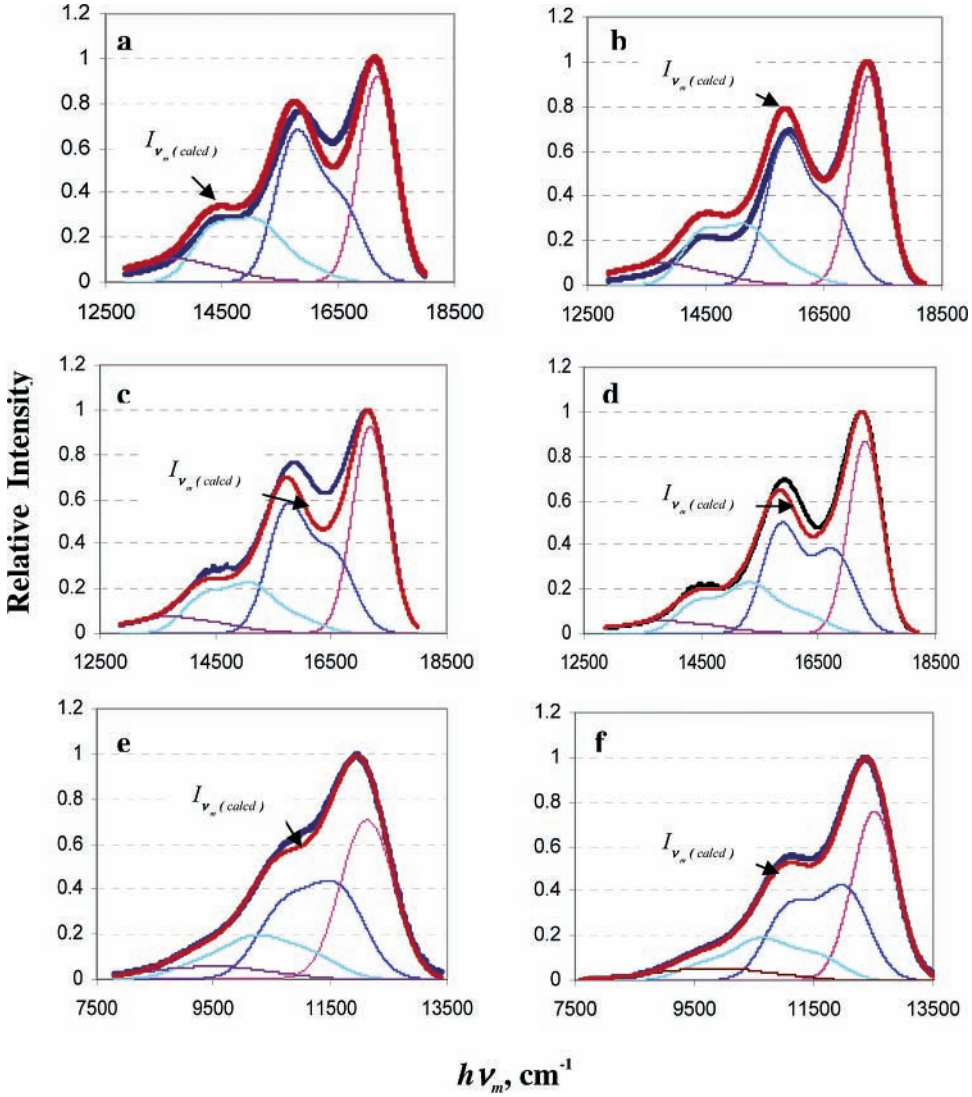

Figure 4. Fittings of resonance-Raman data to the 77 K emission spectra observed in (1:1) DMSO/water, left column, and butyronitrile, right column, for $[Ru(bpy)_3]^{2+}$ (a−d) and $[Ru(NH_3)_4bpy]^{2+}$ (e and f). The observed spectra are the heavy black curves. The fitted spectra, heavy red curves ($I_{\nu_m(calcd)}$), are the convolutions of the fundamental, purple curve, and the sums of the first-order, blue curve, second-order, green curve, and third-order, brown curve, vibronic components; see eqs 11−15. For panels a, b, e, and f, the reorganizational energies are based on the reported resonance-Raman parameters; for panel c the λ_i are assumed to be 1.4 times the values of λ_i for each of the vibrational frequencies, ν_i, reported for $[Ru(NH_3)_4bpy]^{2+}$; for panel d the ratio of λ_i was assumed to be 1.3.

and 12). The latter is an important observation since rR data are only available for a few complexes.

We have assumed that there are no differences in selection rules for vibronic contributions to the emission and the resonance-Raman spectra in C_2 or C_{2v} symmetry, and we have used eqs 11−15 to construct the contributions of the first-, second-, and third-order vibronic components to the emission spectrum as a function of component bandwidth for $[Ru(bpy)_3]^{2+}$ and for $[Ru(NH_3)_4bpy]^{2+}$. The higher order contributions are constructed as the sums of all the harmonics and of all the combination bands of the coupled vibrational modes found in the rR spectra. It is important to observe that the second-order contributions are significant in the 1500 cm^{-1} region of the dominant vibronic feature of both spectra. The failure to include the contributions of the combination bands results in much worse fits. The sum of the contributions of each order of these components is indicated separately in Figure 4.

b. The Ambient Emission Spectrum of $[Ru(bpy)_3]^{2+}$. The ambient emission of this complex is broad and featureless. The component bandwidths seem to be about double those found in the 77 K spectrum, consistent with the temperature difference and eq 1. Our modeling of the emission spectra (described below) demonstrates that a consequence of increases in bandwidth is the increasing importance of second- and third-order vibronic contributions and a shift of the observed emission maximum to lower energies, see Figures 10 and 11. The fundamental obtained from the ambient spectrum by our Grams32 procedure has $h\nu_{max(f)} = 16\,270$ cm^{-1} and $\Delta\nu_{1/2} = 1760$ cm^{-1}. We have used the reported[19] rR parameters to refine these estimates and obtain the parameters reported in Table 1. Adjusting the fundamental to fit the rR parameters increases $h\nu_{max(f)}$ by 1.5% and reduces $\Delta\nu_{1/2}$ by 7.5%, but it results in a 33% reduction of the apparent intensity of this component. This uncertainty in the intensity of the fundamental makes it nearly impossible to assess the vibronic contributions (see eq 2) to the unstructured emission unless other information, such as the rR parameters, is available. It is important to note that Λ_x almost doubles between 77 and 300 K. Our modeling (see below) demonstrates that this is a consequence of the increase of component bandwidths and it does not suggest a temperature dependence of the excited-state distortion.

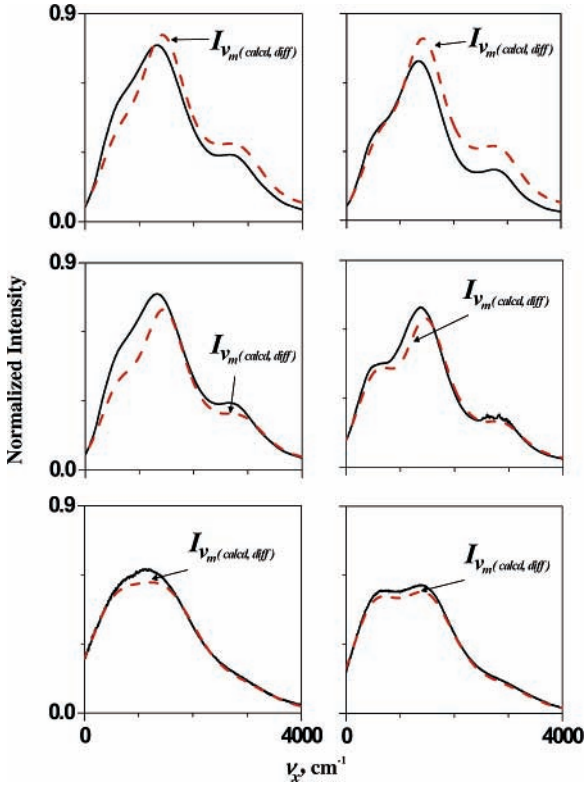

Figure 5. Comparison of the experimental, $I_{\nu_m(\mathrm{exp;diff})}$ (black curves), and calculated, $I_{\nu_m(\mathrm{calcd;diff})}$ (dashed red curves), difference spectra. The fundamental, I_f, used for $I_{\nu_m(\mathrm{exp;diff})} = (I_{\nu_m(\mathrm{spec})} - I_f)$ was obtained from Grams32 fits of the experimental emission spectra and adjusted to fit the rR data; $I_{\nu_m(\mathrm{calcd;diff})}$ was calculated from the resonance-Raman parameters (eq 16). Emission spectra at 77 K obtained in DMSO/water, left column, and butyronitrile, right column. $I_{\nu_m(\mathrm{calcd;diff})}$ for $[Ru(bpy)_3]^{2+}$ based on the reported[19] rR parameters, top row, and with $I_{\nu_m(\mathrm{calcd;diff})}$ for $[Ru(bpy)_3]^{2+}$ based on the reorganizational energies of these parameters adjusted to 1.4 times (middle left) and 1.3 times (middle right) the corresponding values of λ_i of $[Ru(NH_3)_4bpy]^{2+}$. Comparisons of $I_{\nu_m(\mathrm{calcd;diff})}$ and $I_{\nu_m(\mathrm{exp;diff})}$ for $[Ru(NH_3)_4bpy]^{2+}$, bottom.

4. The Evaluation of Procedures and Parameters Used in the Spectral Analysis Using rR-Based Gaussian Vibronic Component Models. We have used the rR parameters for $[Ru(bpy)_3]^{2+}$ and $[Ru(NH_3)_4bpy]^{2+}$ to model the dependence of the observable spectroscopic properties on component bandwidths. We have used the rR parameters for both complexes in order to bracket the variations of emission spectra for the complexes described in this report. This modeling enables us to make bandwidth corrections in order to better evaluate trends in the observed emission spectra.

a. Resonance-Raman-Based Modeling of the Grams32 Deconvolution Procedure. The modeling indicates that there is very little variation in the energy of the fundamental, $h\nu_{f(fit)}$, with $\Delta\nu_{1/2}$. There are larger variations in its intensity, $I_{\nu_m(f;fit)}$, with $\Delta\nu_{1/2}$. These are approximately linear ($r^2 = 0.995$) over the range of $\Delta\nu_{1/2} = 600-1300$ cm^{-1} and for $[Ru(bpy)_3]^{2+}$ and $[Ru(NH_3)_4bpy]^{2+}$ respectively ($\Delta\nu_{1/2}$ in cm^{-1}),

$$[I_{\nu_m(f;fit)} - I_{\nu_m(f)}]/I_{\nu_m(f)} = ((3.25 \pm 0.09) \times 10^{-4})\Delta\nu_{1/2(fit)} - 0.18 \pm 0.01 \quad (17)$$

$$[I_{\nu_m(f;fit)} - I_{\nu_m(f)}]/I_{\nu_m(f)} = ((4.99 \pm 0.17) \times 10^{-4})\Delta\nu_{1/2(fit)} - 0.21 \pm 0.02 \quad (18)$$

The bandwidths of the Grams32 fitted fundamentals vary linearly with the input bandwidths (over the same range as above); the fits for $[Ru(bpy)_3]^{2+}$ and $[Ru(NH_3)_4bpy]^{2+}$ respectively are ($r^2 = 0.995$)

$$\Delta\nu_{1/2}(\mathrm{fit}) = (1.22 \pm 0.03)\Delta\nu_{1/2} - 157 \pm 37 \quad (19)$$

$$\Delta\nu_{1/2}(\mathrm{fit}) = (1.04 \pm 0.01)\Delta\nu_{1/2} - 13 \pm 12 \quad (20)$$

b. Resonance-Raman-Based Modeling of emreps. The envelope of vibronic contributions to an emrep is the sum over the reorganizational energy contributions of all the contributing vibrational modes. Since the vibronic components have significant bandwidths, their contributions to an emrep will also have a significant bandwidth. To compare the emreps of different complexes, it is necessary to correct for any effects of the variations of component bandwidths. To emphasize that the envelopes are the sums of such contributions, we have labeled them as Λ_x; similarly, and because we have made a bandwidth correction, eq 5, we label the vibrational energy axis "$h\nu_x$". The shapes, amplitudes (Λ_x), and energies ($h\nu_x$) of the principal features of these profiles are reproducible, within reasonable error limits (5−10%), in different determinations of the spectra. Changing the energy and width of the fundamental changes the reorganizational energy profile parameters, and this is the principal source of uncertainty in the inferred reorganizational energy contributions (see Appendix A). The uncertainties are much larger for the lower frequency vibrations (for $h\nu_x < 500$ cm^{-1}, the uncertainty in Λ_x is greater than 50% since $\Delta\nu_{1/2}$ is of the order of 1000 cm^{-1} and I_f makes a very large percentage contribution to the observed emission intensity)[64] than for those displaced by more than 1000 cm^{-1} from the maximum of the fundamental (uncertainties of less than about ±15% of Λ_x).[64]

The experimental and calculated emreps are compared in Figure 6. The apparent reorganizational energies are reasonably consistent with those obtained from the experimental spectra: the energy and amplitude of the major vibronic contributions at about 1500 cm^{-1} are reproduced reasonably well (these contributions are reproduced best for the rR parameters of $[Ru(bpy)_3]^{2+}$ adjusted to be in a constant ratio to those of [Ru-

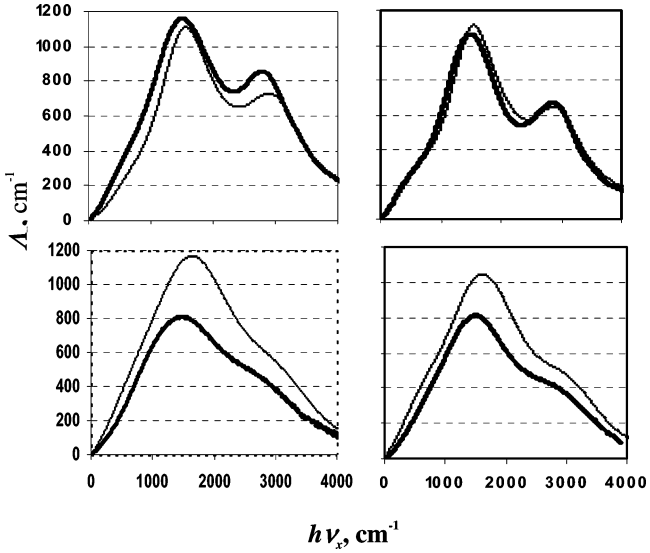

Figure 6. Comparison of emreps based on experimental (77 K) emission spectra, heavy line, to those based on the best fit of resonance-Raman data, light line for $[Ru(bpy)_3]^{2+}$, top, and $[Ru(NH_3bpy]^{2+}$, bottom, in DMSO/water, left, and butyronitrile, right. Most of the amplitude differences of the calculated and experimental emreps arise from the differences between $I_{max(f)}$ as evaluated from the Grams32 fitting and that with the intensity adjusted to accommodate the rR data.

TABLE 3: Parameters Calculated for Attenuation Plots[a]

Ru^{II} complex [ligands]	DMSO/water							butyronitrile						
	$\Delta\nu_{1/2}$	$\Lambda_{x(\text{obsd})}$	$\Lambda_{1st(vx)}$[b]	$\Lambda_{1st(corr)}$[c]	$\Lambda_{x(corr)}$	$h\nu_{max(f)}$[d]	$n_e\alpha_{eff}{}^2$[e]	$\Delta\nu_{1/2}$	$\Lambda_{x(\text{obsd})}$	$\Lambda_{1st(vx)}$[b]	$\Lambda_{1st(corr)}$[c]	$\Lambda_{x(corr)}$[d]	$h\nu_{f(max)}$	$n_e\alpha_{eff}{}^2$[e]
$[(bpy)_3]$	680	1160	970	970	1160	17220	0.36 ± 0.05	640	1050	920	920	1050	17310	0.36 ± 0.08
$[en(bpy)_2]$	780	1000	780	750	960	15060	0.47 ± 0.06	720	880	720	700	850	15160	0.47 ± 0.10
$[(NH_3)_2(bpy)_2]$	910	990	770	700	900	14640	0.49 ± 0.07	780	860	710	670	810	14700	0.50 ± 0.10
$[([14]aneN_4)bpy]$	950	850	600	510	740	14010	0.54 ± 0.07	890	810	580	500	710	14030	0.54 ± 0.11
$[(en)_2bpy]$	1030	850	600	480	700	12880	0.64 ± 0.09	890	780	560	480	680	13050	0.63 ± 0.13
$[(NH_3)_4bpy]$	1110	810	580	440	640	12090	0.73 ± 0.10	920	800	570	480	690	12420	0.70 ± 0.15
$[(d_4\text{-en})(bpy)_2]$	780	990	770	740	960	15080	0.47 ± 0.06							
$[(ND_3)_2(bpy)_2]$	910	980	770	700	890	14660	0.49 ± 0.07							
$[(d_4\text{-}[14]aneN_4)bpy]$	970	850	600	500	730	13990	0.54 ± 0.07							
$[(d_4\text{-en})_2bpy]$	1040	840	590	480	690	12890	0.64 ± 0.09							
$[(ND_3)_4bpy]$	1130	800	570	430	620	12010	0.73 ± 0.10							

[a] All energies in cm^{-1}. [b] For $[Ru(bpy)_3]^{2+}$: $\Lambda_{1st(vx)} = (0.47 \pm 0.03)\Lambda_x + (426 \pm 44)$. For $[Ru(Am)_4(bpy)]^{2+}$: $\Lambda_{1st(vx)} = (0.454 \pm 0.02)\Lambda_x + (213 \pm 20)$. For $[Ru(Am)_2(bpy)_2]^{2+}$: $\Lambda_{1st(vx)} = (0.46)\Lambda_x + (319)$. [c] For $[Ru(Am)_4(bpy)]^{2+}$: $\Lambda_{1st(corr)} = \Lambda_{1st} - \{0.32[\Delta\nu_{1/2}([Ru(Am)_4(bpy)]^{2+}) - \Delta\nu_{1/2}([Ru(bpy)_3]^{2+})]\}$. For $[Ru(Am)_2(bpy)_2]^{2+}$: $\Lambda_{1st(corr)} = \Lambda_{1st} - \{0.32[\Delta\nu_{1/2}([Ru(Am)_2(bpy)_2]^{2+}) - \Delta\nu_{1/2}([Ru(bpy)_3]^{2+})]\}$. [d] Appendix A, eqs A2, A3, and A4. [e] Apparent value of $n_e\alpha_{eg}{}^2$ based on eq 26: $n_e\alpha_{eg}{}^2 = 1 - \Lambda_{1st(corr)}/\Lambda_{1st(corr)}{}^o$. $\Lambda_{1st(corr)}{}^o = 1370\ cm^{-1}$ in DMSO/water and $1330\ cm^{-1}$ in butyronitrile (see Table 4).

TABLE 4: Reorganizational Energy Attenuation Parameters for $[Ru(Am)_{6-2n}(bpy)_n]^{2+}$ Complexes

solvent	complexes selected[a]	k[b]	intercept (Λ^o),[b,c] cm^{-1}	$a \times 10^9$ [b,c]
DMSO/water	all (NH, ND)[d]	x(obsd)	1420 ± 70	0.068 ± 0.009
		1st	1240 ± 100	0.084 ± 0.015
		1st(corr)	1370 ± 110	0.11 ± 0.01
		x(corr)	1580 ± 90	0.093 ± 0.010
	NH_3, ND_3[e]	x(obsd)	1470 ± 40	0.068 ± 0.006
		1st	1300 ± 50	0.083 ± 0.008
		1st(corr)	1420 ± 80	0.10 ± 0.01
		x(corr)	1610 ± 70	0.091 ± 0.008
butyronitrile	all (NH)[f]	x(obsd)	1250 ± 100	0.062 ± 0.017
		1st	1240 ± 130	0.090 ± 0.020
		1st(corr)	1330 ± 150	0.11 ± 0.02
		x(corr)	1370 ± 120	0.084 ± 0.018
	NH_3[g]	x(obsd)	1270 ± 160	0.060 ± 0.025
		1st	1250 ± 110	0.086 ± 0.018
		1st(corr)	1350 ± 130	0.10 ± 0.02
		x(corr)	1380 ± 170	0.080 ± 0.024

[a] $[Ru(Am)_{6-2n}(bpy)_n]^{2+}$ complexes in Table 1; NH and ND refer to the respective isotopometers. [b] For $\Lambda_k = \Lambda^o - a\Lambda^o/(h\nu_{max(f)})^2$. [c] R^2 from 0.88 to 0.98. [d] All of $[Ru(Am)_{6-2n}(bpy)_n]^{2+}$ complexes ($n = 1-3$ and Am = NH, ND), see Table 3. [e] $[Ru(bpy)_3]^{2+}$, $[Ru(NH_3/ND_3)_2(bpy)_2]^{2+}$, and $[Ru(NH_3/ND_3)_4(bpy)]^{2+}$ complexes. [f] All of $[Ru(Am)_{6-2n}(bpy)_n]^{2+}$ complexes ($n = 1-3$ and Am = NH), see Table 3. [g] $[Ru(bpy)_3]^{2+}$, $[Ru(NH_3)_2(bpy)_2]^{2+}$, and $[Ru(NH_3)_4(bpy)]^{2+}$ complexes.

$(NH_3)_4bpy]^{2+}$). Even at $1500\ cm^{-1}$, the second-order vibronic components contribute 10−35% to Λ_x. Nevertheless, the ratios of emreps of different compounds are relatively weakly dependent on the bandwidth (see Figure 3), and useful information about the differences in multimode excited state distortions of a series of complexes can be obtained, with relatively small corrections, from the emreps of complexes with component bandwidths less than about $1500\ cm^{-1}$.

The evaluation of the attenuation of vibronic sidebands by eq 4 is based on the first-order vibronic components. One would expect greater attenuation ($\sim[1 - 4\alpha_{eg}{}^2]^2$) of second-order components as expressed in eq 13, and the evaluation of the differences of band shape must take account of the different contributions of first- and second-order components. Since the key parameters are functions of the bandwidth, we can use the rR modeling to estimate that part of $\Lambda_{x(max)}$ that arises only from first-order vibronic contributions at any specified value of the bandwidth. The attenuation effects are most easily interpreted in terms of the sum of first-order component contributions, Λ_{1st}, but each compound has a different intrinsic bandwidth, and the reorganizational parameters are functions of the bandwidth; for example, from the modeling for $[Ru(bpy)_3]^{2+}$ and $[Ru(NH_3)_4bpy]^{2+}$, respectively,

$$\Lambda_{1st(cor)} = (0.33 \pm 0.05)\,|\partial\Delta\nu_{1/2}| + 742 \pm 48 \quad (21)$$

$$\Lambda_{1st(cor)} = (0.32 \pm 0.005)\,|\partial\Delta\nu_{1/2}| + 382 \pm 5 \quad (22)$$

Equations 21 and 22 imply that $\Lambda_{1st(cor)} = (0.32)\,|\partial\Delta\nu_{1/2}| + 562$ for $[Ru(Am)_2(bpy)_2]^{2+}$.

For the $600 \le \Delta\nu_{1/2} \le 1500\ cm^{-1}$ range of bandwidths, the modeling for $[Ru(bpy)_3]^{2+}$ gives the first-order contributions ($r^2 = 0.99$): For $[Ru(bpy)_3]^{2+}$ (evaluated at $\nu_d = 1493\ cm^{-1}$), $I_{lst}/I_{total} = 0.957 \pm 0.003 - ((1.71 \pm 0.04) \times 10^{-4})\Delta\nu_{1/2}$; and for $[Ru(NH_3)_4bpy]^{2+}$ (evaluated at $\nu_d = 1481\ cm^{-1}$), $I_{lst}/I_{total} = 0.781 \pm 0.004 - ((1.16 \pm 0.03) \times 10^{-4})\Delta\nu_{1/2}$. Bandwidth corrections can be made in either Λ_{1st} or Λ_x. The apparent attenuations are slightly larger (10−25%) when the bandwidth corrections are made in Λ_{1st}, and this approach has been used for the parameters in Tables 3 and 4.

The corrections used in these tables for $[Ru(bpy)_3]^{2+}$ and $[Ru(NH_3)_4bpy]^{2+}$ respectively evaluated at the emrep maxima are,

$$\Lambda_{1st(\nu x)} = (0.470 \pm 0.03)\Lambda_{x(max)} + (426 \pm 44) \quad (23)$$

$$\Lambda_{1st(\nu x)} = (0.454 \pm 0.02)\Lambda_{x(max)} + (213 \pm 20) \quad (24)$$

From eqs 23 and 24 we infer for $[Ru(Am)_2(bpy)_2]^{2+}$: $\Lambda_{1st(\nu x)} = (0.46)\Lambda_{x(max)} + 319$.

When the complexes compared differ in bandwidth a correction for this difference must be made. We have made the corrections for bandwidths in the range of $\Delta\nu_{1/2(fit)} = 600-1500\ cm^{-1}$ based on,

$$\Lambda_{k(cor)} = \Lambda_k - \frac{d\Lambda_k}{d\Delta\nu_{1/2}}\,|\partial\Delta\nu_{1/2}| \quad (25)$$

and eqs 21 and 22; $\partial\Delta\nu_{1/2}$ is the difference between the reference and observed bandwidths and the subscript $k = x$, 1st, etc.

Based on these corrections, and assuming that the distortion of the bpy ligand is simply proportional to the amount of charge that is delocalized between the metal and the ligand, the different bpy−ligand distortions of the complexes give rise to differences in attenuation of the vibronic contributions. For purposes of experimental correlations this is represented as,

$$\Lambda_{1st} \cong \Lambda_{1st}{}^o(1 - n_e\alpha_{eff}{}^2) \quad (26)$$

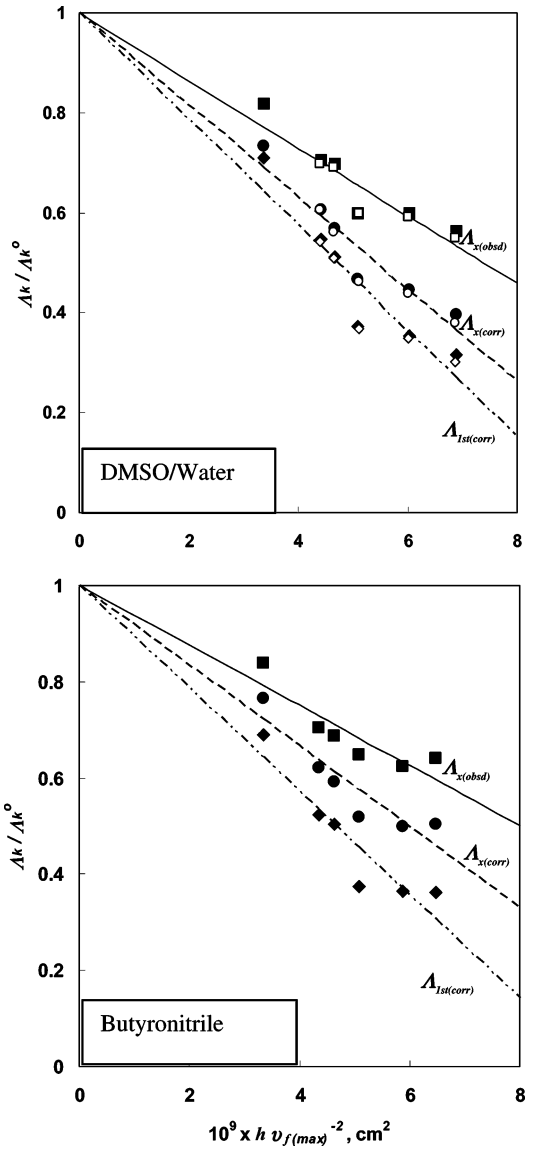

Figure 7. Attenuation of bipyridine ligand reorganizational energies of $[Ru(Am)_{6-2n}(bpy)_n]^{2+}$ complexes in DMSO/water (top) and butyronitrile (bottom) glasses at 77 K. Based on $\Lambda_k/\Lambda_k^o = (1 - n_e\alpha_{eff}^2)$. The squares, circles, and diamonds are $\Lambda_{x(obsd)}$, $\Lambda_{x(corr)}$ and $\Lambda_{1st(corr)}$, respectively. The filled symbols are the NH complexes of $[Ru(Am)_{6-2n}(bpy)_n]^{2+}$, $n = 1-3$, and the open symbols are the ND isotopomers of $[Ru(Am)_{6-2n}(bpy)_n]^{2+}$, $n = 1-2$. The data are from Table 3; the parameters for the least-squares fits are summarized in Table 4. $\Lambda_{x(obsd)}$ is obtained from emreps generated with $I_{f(max)}$ from the Grams32 fit; $\Lambda_{x(corr)}$ is based on eqs A2−A4; and $\Lambda_{1st(corr)}$ is based on eqs 21−25. The sequence of complexes from top to bottom in each figure is the same as in Figure 8.

Where in the simplest two state model and for $\alpha_{eff}^2 = \alpha_{eg}^2 < 0.1$, $n_e = 4$ (eqs 3 and 4), Λ_k^o at a specific energy (e.g., 1500 cm^{-1}) and bandwidth is the sum of first, second, and higher order reorganizational energy contributions in the absence of configurational mixing (note that the intercept contains substantial bandwidth and other contributions and does not have a simple interpretation), and α_{eg}^2 is the fraction of electron density delocalized in the MLCT excited state. Equation 26 provides a reasonable correlation for the values of Λ_k obtained for the $[Ru(Am)_{6-2n}(bpy)_n]^{2+}$ complexes employed in this study as demonstrated in Figure 7; values of $\Lambda_{x(max)}$, both the values directly inferred from the experimental spectrum ($\Lambda_{x(obsd)}$) and the values corrected for differences in bandwidth ($\Lambda_{x(corr)}$), are included in this figure for comparison. The correlation parameters are summarized in Table 4. The respective values of Λ_{1st} estimated for $[Ru(NH_3)_4bpy]^{2+}$ and $[Ru(bpy)_3]^{2+}$ in butyronitrile are 570 ± 40 and 920 ± 30 cm^{-1} (in DMSO/water, $\Lambda_{1st} = 570 \pm 40$ and 970 ± 35 cm^{-1}); the bandwidth correction (eqs 22 and 26) gives $\Lambda_{1st(corr)} = 480$ (430) cm^{-1} for $[Ru(NH_3)_4bpy]^{2+}$. This indicates that the first-order reorganizational energy components for the bpy distortion modes of $[Ru(NH_3)_4bpy]^{2+}$ average about 50% of those of $[Ru(bpy)_3]^{2+}$ (the ratio is $(1.95 \pm 0.15)^{-1}$). The attenuation effect appears to be the same in the two frozen matrices. This is a very large effect. It is an effect that is reflected in the modeling by the observation that first-order contributions constitute about 86% of the intensity of $[Ru(bpy)_3]^{2+}$ in the bandwidth range observed experimentally but only 65% for $[Ru(NH_3)_4bpy]^{2+}$; when corrected for bandwidth this gives a reorganizational energy ratio of about 1.5. Interpreted in terms of eq 4, a 1.5- to 2-fold attenuation implies a very large amount of configurational mixing for the $[Ru(NH_3)_4bpy]^{2+}$ complex in the region of its excited-state PE minimum.

The considerations in this section are based on the fits of the respective rR data to the emission spectra of $[Ru(bpy)_3]^{2+}$ and [$[Ru(NH_3)_4bpy]^{2+}$. These considerations indicate that in order to evaluate the changes in the vibronic contributions to the emission spectra of these complexes it is necessary to (i) evaluate the fundamental (e.g., based on the Grams32 fits, as described above), (ii) correct the amplitude of the deconvoluted fundamental (e.g., with an interpolation based on eqs 17 and 18), (iii) use the corrected fundamental to generate an emrep, (iv) estimate $\Lambda_{x(1st)}$ (e.g., with an interpolation based eqs 21 and 22), and (v) correct for differences in $\Delta\nu_{1/2}$ with an interpolation based on eqs 23−25. Since all of the parameters of interest can be parametrized as functions of $\Delta\nu_{1/2}$, some of these steps may be bypassed (as in eqs 23 and 24). The evaluation of reorganizational parameters for the complexes studied is summarized in Table 3.

6. Excited-State Lifetimes. The luminescence decays of these complexes were fitted well by single exponentials. The luminescence decays of $[Ru(NH_3)_4bpy]^{2+}$, with a lifetime of about 25 ns, were close to the detection limits of our system; limits were determined by analog/digital conversion, trigger jitter, and laser pulse width (with the averaging of >50 signals, probably ±5−10 ns).

7. The Contributions of Very High Frequency (ν_h > 2000 cm^{-1}) Vibrational Modes. We have searched for the contributions of N−H and C−H stretching modes to the emission spectrum. These contributions appear to be very small. The details will be treated elsewhere.[78] Some of the observations on the perdeuterio−am(m)ine complexes are included here in order to improve the statistics in the evaluation of vibronic attenuation (Figure 7).

Discussion

We have found that the energies and band shapes of the 77 K frozen solution emission spectra of a series of $[Ru(Am)_{6-2n}(bpy)_n]^{2+}$ complexes vary markedly as the number of am(m)ines (Am) is changed: (1) the emission energies decrease as n increases; (2) the intrinsic, component bandwidth, $\Delta\nu_{1/2}$, increases in this same order; and (3) the relative amplitudes of low-energy contributions to the emission band are markedly attenuated as the energy of the fundamental component ($h\nu_{max(f)} = E^{0'0} - \chi_s$) decreases. The changes in band shape can be addressed in terms of the expected changes in configurational mixing and/or of electronic delocalization with the differences in ground- and excited-state energies. Thus, the intensities of the emission at energies smaller than ($h\nu_{max(f)}$ −

$\Delta\nu_{1/2}$) are attributed to vibronic contributions that arise from bipyridine ligand distortions in the MLCT excited states, and these contributions can be represented as the sum of the intensity contributions of progressions of vibrational modes that correlate with the excited-state distortion. These vibronic contributions decrease in amplitude with increases in ground-state/excited-state configurational mixing, and the configurational mixing increases with decreases in the energy difference of these states. Very large variations in configurational mixing are implied by the very substantial attenuation of vibronic contributions to the emission through the series of complexes.

We have evaluated the emission band shapes in terms of reorganizational energy profiles (emreps). We have used a model based on the resonance-Raman lines reported for $[Ru(bpy)_3]^{2+}$ [19] and $[Ru(NH_3)_4bpy]^{2+}$ [18] and Gaussian band shapes for each of those vibronic components in our spectral analysis. A number of important aspects of the determinations of $E_{max(f)}$ and of the emreps need to be discussed before we address the vibronic attenuation and its implications.

1. The Evaluation of the $[Ru(Am)_{6-2n}(bpy)_n]^{2+}$ MLCT Excited-State Energies. We have used Gaussian deconvolutions by means of the Grams32 program to obtain the energies of the fundamentals. The rR-based modeling indicates that this approach underestimates the energy of the fundamental by about 0.2% for $[Ru(bpy)_3]^{2+}$ and by about 1% for $[Ru(NH_3)_4bpy]^{2+}$. Deconvolutions of the broad and unstructured ambient solution emission spectra of these complexes are far less reliable, but the value of $E_{max(f)} = 16\,530$ cm^{-1} obtained by fitting the emission of $[Ru(bpy)_3]^{2+}$ in ambient DMSO/water solutions using resonance-Raman parameters to model the band shape (see Table 1) is in excellent agreement with the value of $E_{max(f)} = 16800 \pm 200$ cm^{-1} obtained in water by photoacoustic microcalorimetry.[79,80]

The energies of MLCT excited states of polypyridyl complexes are often based on correlations with electrochemical oxidations and reductions in ambient solutions.[23] While Figure 8 demonstrates that this provides a very good correlation for the complexes considered here ($r^2 = 0.97$), $E_{max(f)}$ and $F\Delta E_{1/2}$ (values summarized in Table S3, Supporting Information)[72] are not simply (1:1) correlated: $F\Delta E_{1/2} > E_{max(f)}$ and the differences vary systematically from 3.7×10^3 cm^{-1} for $[Ru(bpy)_3]^{2+}$ to 5.3×10^3 cm^{-1} for $[Ru(NH_3)_4bpy]^{2+}$. Some of these differences must arise from the differences in the experimental conditions (fluid and frozen solutions for $\Delta E_{1/2}$ and $E_{max(f)}$, respectively; when both measurements are in fluid solution, the discrepancy for $[Ru(bpy)_3]^{2+}$ is about 700 cm^{-1} larger), and in the different ways in which the solvent affects the electrochemical and spectroscopic measurements.[3] A substantial part of these differences must also arise from systematic variations in the exchange energy, K_{exch} (i.e., for $2K_{exch} \cong$ the singlet/triplet MLCT excited-state energy difference), which is of the order of a few thousand wavenumbers for these complexes and is expected to be much larger for $[Ru(NH_3)_4bpy]^{2+}$ than for $[Ru(bpy)_3]^{2+}$,[33] and larger for the triplet MLCT excited states than for the doublet states generated electrochemically.[3,59,60] The electrochemical measurements do not provide a good estimate of MLCT excited-state energies, or even of the variations in those energies in these complexes. However, the good empirical correlations between $E_{max(f)}$ and $\Delta E_{1/2}$ that result from systematic variations in parameters for a series of closely related complexes are qualitatively useful in verifying the assignments of optical transitions.

2. Some Implications of the rR Modeling. Overall the rR-based modeling indicates that the 77 K spectral band shapes of these complexes can be used to obtain useful information about the variations in vibronic intensities and, consequently, about the differences in excited state distortions in the series of complexes. The modeling also demonstrates how strongly the vibronic contributions to the observed spectrum vary with spectral bandwidth. Several specific points are important here:

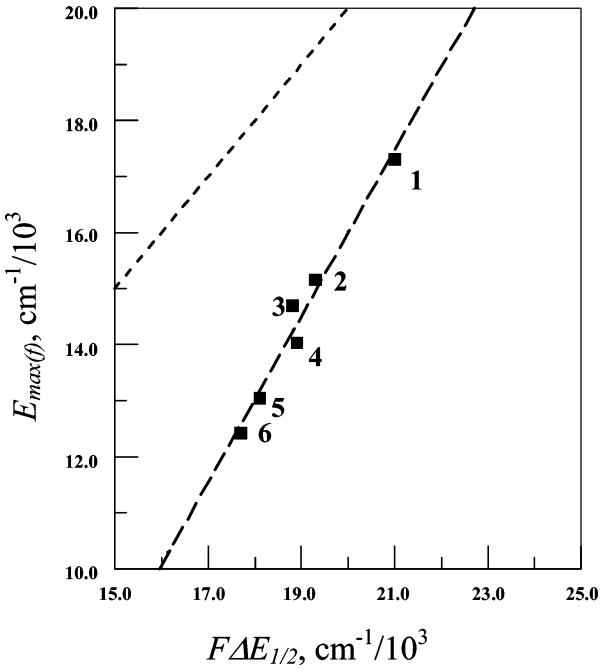

Figure 8. Correlation $E_{max(f)}$, evaluated by Grams32 deconvolution of the 77 K emission spectra in 77 K butyronitrile solutions (Table 1), with $\Delta E_{1/2}$, determined in ambient acetonitrile solutions: $[Ru(bpy)_3]^{2+}$, 1; $[Ru(en)(bpy)_2]^{2+}$, 2; $[Ru(NH_3)_2(bpy)_2]^{2+}$, 3; $[Ru([14]aneN_4)bpy]^{2+}$, 4; $[Ru(en)_2bpy]^{2+}$, 5; $[Ru(NH_3)_4bpy]^{2+}$, 6. Least-squares line (dashed): $E_{max(f)} = (1.48 \pm 0.13)\Delta E_{1/2} - (13.6 \pm 2.5)$, cm^{-1}/10^3. For purposes of comparison, the upper dashed line is based on $E_{max(f)} = \Delta E_{1/2}$.

a. Spectral Fittings. The rR data for $[Ru(NH_3)_4bpy]^{2+}$ provide an excellent fit of the vibronic contributions to the observed spectrum, Figures 4 and 5. The fits of the rR data for $[Ru(bpy)_3]^{2+}$ to the observed spectrum are improved if the reorganizational energies for the bpy vibrations are held in a constant ratio to those of the corresponding vibrations of $[Ru(NH_3)_4bpy]^{2+}$, Figures 4 and 5. Since the rR parameters are obtained for the Franck−Condon singlet excited states of these complexes, the fits to the 77 K emission spectra are probably all better than one might have expected.[41,43]

b. Component Bandwidth Contributions to the Overall Spectral Features. While the energy and bandwidth of the Grams32-deconvoluted fundamentals are only very weakly dependent on bandwidth, the apparent intensity of this evaluation of the fundamental does increase significantly as the bandwidth increases. This results in very large uncertainties in the evaluation of the vibronic contributions with small vibrational energies ($\nu_d < 500$ cm^{-1}) and the evaluation is based only on the observed spectrum and the deconvoluted fundamental. We set the intensity of the emission maximum equal to one in our spectral analysis, so increases of component bandwidth result in dramatic changes of the band shape and a shift of the energy of the emission maximum as illustrated in Figure 10. For bandwidths in the range observed for the complexes discussed here (700−1300 cm^{-1}), the vibronic "band" at an energy about 1500 cm^{-1} lower than $E_{max(f)}$ is a composite of the contributions of overlapping first-order components (83−74% for $[Ru(bpy)_3]^{2+}$ and 72−63% for $[Ru(NH_3)_4bpy]^{2+}$) and second-order components (17−24% and 28−34%, respectively). Obviously,

the representation of this spectral feature by a single high frequency vibronic component would greatly misrepresent the excited state distortion and result in an incorrect evaluation of the vibronic contributions to the emission spectra. We have found that single high frequency vibrational mode models give very poor fits to the emission spectra, especially in the long wavelength regions.

c. The Evaluation of Variations in the Vibronic Contributions Through the Series of Complexes. Since the construction of emreps depends on the ratio of intensities, eq 3, and since all of the intensity quantities increase with component bandwidth, the variations of emrep amplitudes are less sensitive to changes in bandwidths than are the spectral intensities. On the other hand, the substantial overlapping of first-, second-, and third-order components can complicate the interpretation of changes in emrep amplitudes. All of the pertinent parameters are functions of the bandwidth (see the Results section and Appendix A), and the rR-based modeling indicates that the net first-order vibronic contributions to $\Lambda_{x(\max)}$ can be estimated using eqs 23 and 24. To evaluate the attenuation of reorganizational energies, we have corrected for the effects of the bandwidth differences between compounds using eqs 21, 22, and 26.

3. The Attenuation of Vibronic Sidebands. *a. General.* We have explored the quantitative evaluation of the attenuation of the spectral contributions of the bpy vibrational modes (illustrated in Figure 2) of the $[Ru(Am)_{6-2n}(bpy)_n]^{2+}$ complexes using (1) emrep maxima for these complexes and (2) the emrep maxima with rR modeling based corrections for bandwidth differences and (3) with rR modeling based corrections for the overlapping contributions of first- and second-order vibronic envelopes. The results of this analysis are illustrated in Figure 7 and summarized in Tables 3 and 4. On the average, the bpy vibrational reorganizational energy contributions of $[Ru(NH_3)_4bpy]^{2+}$ vary from 49% (for $\Lambda_{1st(corr)}$) to 60% (for $\Lambda_{x(corr)}$) of those for $[Ru(bpy)_3]^{2+}$; α_{eg} is larger for the tetraammine complex, corresponding to appreciably greater configurational mixing, and eqs 4 and 26 predict greater vibronic attenuation for this complex.

The attenuation implied in Figure 7 is very large. However, such substantial attenuation with the decreases of the excited state/ground state energy difference contrasts with the apparently very good fit of the emission spectrum of $[Ru(NH_3)_4bpy]^{2+}$ to the rR data since the difference of the ambient absorption maximum of about 19×10^3 cm^{-1} and $h\nu_{max(f)} = (12 \text{ to } 13) \times 10^3$ cm^{-1} at 77 K is comparable to the range of emission energies represented in Figure 7, and this implies that there should be a considerably greater attenuation of the vibronic contributions in the emission spectrum. Some very general aspects of these complicated issues are discussed here.

b. Possible Interpretations of the Attenuation Parameter $n_e\alpha_{eff}^2$. Equation 4 is most readily interpreted in terms of a two-state system in which the ground and excited states have the same spin multiplicity. The emitting Ru/bpy MLCT excited states have significant triplet spin character and some deviations from the simple two-state limit might be expected. The basic elements of a two-state model can be preserved if one considers only configurational mixing between the ^{3}MLCT excited state and the ground state, with the electronic matrix element represented as,

$$H_{eg} \cong (H_{so}/E_{ST})H_{ge} \tag{27}$$

where H_{so} is the matrix element for spin−orbit coupling between the ^{1}MLCT and ^{3}MLCT excited states, $E_{ST} \cong 2K_{exch}$, and H_{ge} is the matrix element for ^{1}MLCT/ground-state electronic coupling (estimated to be about 7000 cm^{-1}).[3] From Table 3, $\Lambda_{1st(corr;B)} - \Lambda_{1st(corr;A)} = 530$ cm^{-1} (where the subscripts (A) and (B) designate parameters for the complexes $[Ru(NH_3)_4bpy]^{2+}$ and $[Ru(bpy)_3]^{2+}$, respectively, for data obtained in DMSO/water), or $n_e(\Delta\alpha_{eff}^2) \cong 0.37$. This corresponds to very substantial attenuation, and it suggests that at least some of these complexes fall outside the range of applicability of eq 4 ($\alpha_{ge}^2 \leq \sim 0.1$). For $H_{eff} \approx 7000$ cm^{-1} the values of $n_e(\Delta\alpha_{eff}^2) \cong 0.37$ and $a \cong 1 \times 10^8$ cm^2 from Table 4 imply that $n_e \approx 2$; alternatively for the limit represented in eq 4, $n_e \approx 4$ leads to $H_{eff} \approx 5000$ cm^{-1}. Since the rR data probe the Franck−Condon excited state for absorption, and since the respective differences in vertical excited- and ground-state energies are about 19 000 and 13 000 cm^{-1} for the absorption and emission maxima of $[Ru(NH_3)_4bpy]^{2+}$, respectively, it is interesting to note that the effective values of $n_e \cong 2$ for the emission and $n_e \cong 4$ for the spin-allowed absorption are consistent with the large attenuation inferred from Figure 7 and with the similarities of attenuation for emission and absorption implied by the fits of rR data in Figures 4 and 5 (a value of $H_{ge} \cong 7000$ cm^{-1} results in about a 10% larger vibronic contribution at 1500 cm^{-1} for absorption than for emission). Since $H_{eg} < H_{ge}$, the equivalent of eqs 4 and 26 for the emission in frozen solutions should be written[60]

$$\Lambda_k \cong \Lambda_k^{\circ}(1 - 2\alpha_{ge}^{\ 2} - 2\alpha_{eg}^{\ 2} + ...) \tag{28}$$

A very approximate value of $H_{eg} \approx 3300$ cm^{-1} results for $H_{ge} \cong 7000$ cm^{-1} and $E_{ST} \approx 4000$ cm^{-1}. However, the magnitude of the attenuation of the vibronic contributions to the emission spectra may be too large to be accommodated by the simple perturbation theory arguments used here and higher order contributions to eqs 26 and 28 should be taken into account.

The data for the $[Ru(bpy)_3]^{2+}$ complex are consistently above the correlation lines in Figure 7, and this implies slightly less attenuation than expected for this complex. This deviation may be a consequence of MLCT/MLCT′ configurational mixing (mentioned above) and we will try to address this in future studies. Nevertheless, the very large attenuation of the vibronic contributions to the emission of $[Ru(NH_3)_4bpy]^{2+}$ indicates that there is a great deal of configurational mixing between the MLCT excited state and the ground state of this complex, and that this results in the relatively small reorganizational parameters. The higher order terms in eq 26 are of the order of α_{ij}^4 and have the opposite sign from the α_{ij}^2 terms. This might account for the relatively small variations among the Λ_k for the $[Ru(Am)_4bpy]^{2+}$ complexes. These issues and other consequences of such extensive configurational mixing will be explored elsewhere.

4. Some Implications for Interpretation of the Nonradiative Relaxation Rate Constants. Nonradiative rate constants can be treated in the nonadiabatic limit with equations of the same general form as the equations used to describe the emission;[12,25] thus, in the semiclassical limit (κ_{el} is an electronic transmission coefficient and ν_{eff} is the frequency of correlated nuclear motions),[54]

$$k_{nr} \cong \kappa_{el}\nu_{eff}\kappa_{nu} \tag{29}$$

the nuclear transmission coefficient (κ_{nu}) = (FC). In applications of equations of the general form of eq 29 to the estimation of 77 K rate constants, the exponential factor in eq 7 behaves approximately as a delta function since the denominator in the exponential is very small compared to $E_{max(f)}$. This leads to an isoenergetic crossing from the MLCT excited state to the ground state that requires the depositing of the excited-state energy,

$E^{0'0}$, in a very large number of vibrational quanta. For the highest energy vibration reported in the rR studies of $[Ru(NH_3)_4bpy]^{2+}$, $j \approx E_{max(f)}/h\nu_i$ must be greater than or equal to 7 (Tables 2 and S4[72]). This can be compared to the fitting of the emission spectra to the rR data using eqs 11−15, which required the calculation of over 10^3 third-order contributions ($j = 3$ in eqs 6−9) using eq 14. There will be a vastly larger number of terms contributing to (*FC*) when $j = 7$. The delta function behavior of the exponential factor of (*FC*), mentioned above, and the very small magnitudes for the contributions for $j > 4$ of terms with $S_i \ll 1$ (see Tables 2 and S4) will limit the importance of most of the possible vibrational relaxation channels, but there are still a very large number of vibrational relaxation channels in which this energy can be deposited. Thus, vibrational combinations such as $(7\nu_5 + \nu_{17})$, $(7\nu_6 + \nu_8)$, $(7\nu_7)$, $(6\nu_7 + \nu_5)$, $(6\nu_7 + \nu_{11} + \nu_{15})$, etc. should contribute to the overall relaxation probability. As a consequence, the sum of the probabilities of all the combinations of contributing vibrational channels can be large even if the probability of relaxation in any one channel is very small. Although no single channel can dominate the relaxation process, the higher powers of $(S_7)^j/j!$ for $\nu_7 = 1481$ cm^{-1} are large relative to those of the other vibrational modes in Table 2 (see Table S4).[72] Nevertheless, one expects a very large number of vibrational relaxation channels that combine several relatively high-frequency distortion modes, such as ν_7, which have relatively large values of S_m with a few lower frequency modes which also have relatively large values of S_k to make significant contributions to k_{nr}. The overall contributions can be approximately formulated

$$k_{nr} \approx \kappa_{el(ave)}\nu_{eff(ave)} \sum_k \left[\frac{(\sum_m S_m)^k \, e^{-S_m}}{k!}\right] \delta_{E_\rho, \sum_m k_m h\nu_m} \quad (30)$$

where $k = \sum_m^{\text{all modes}} k_m$ is the number of vibrational quanta in the relaxation channel. Thus, it is surprising that there is a rough empirical correlation between k_{nr}, $S_x = (\Lambda_{x(max)}/h\nu_{x(max)})$, and j the largest integer less than $(h\nu_{max(f)}/h\nu_{x(max)})$,

$$k_{nr}/s^{-1} \approx ((3 \pm 2) \times 10^{14})\left[\frac{S_x^{\,j}}{j!}\right] e^{-S_x} \quad (31)$$

This correlation is equivalent to assuming that a single vibrational mode of frequency $\nu_{x(max)}$ with a vibrational reorganizational energy $\Lambda_{x(max)}$ determines the back electron-transfer kinetics, and that at 77 K the exponential factor in (*FC*) is approximately one (for reasons noted above). For a single contributing vibrational mode (k) and for $E^{0'0} \gg h\nu_k$, eq 30 can be put in the very simple form[45]

$$k_{nr} = Ae^{-\gamma_x(E_{max(f)}/h\nu_x)}, \qquad \gamma_x = \ln(E_{max(f)}/\Lambda_x) - 1 \quad (32)$$

where we treat the preexponential factor as an adjustable empirical parameter. The correlation of k_{nr}, $\Lambda_{x(max)}$ and $h\nu_{x(max)}$ based on eq 32, Figure 9, is slightly better than that based on eq 30; the least-squares value of $A \approx (3 \pm 2) \times 10^{13}$ s^{-1}. Since a single mode approach does not properly represent the emission spectrum, it is not surprising that eqs 31 and 32 (with $A \approx (3 \pm 2) \times 10^{13}$ s^{-1}) both overestimate the ambient value of k_{nr} for $[Ru(bpy)_3]^{2+}$ by 2 to 3 orders of magnitude even when the values of $\Lambda_{x(max)}$ and $h\nu_{x(max)}$ are based on fitting the ambient spectrum to the resonance Raman parameters. With respect to the details of the fitting, this discrepancy arises largely because the resulting value of $h\nu_{x(max)}$ is so large, as a consequence of the much larger bandwidth, and j is relatively small. The more general point is that a single vibrational mode model of inverted region electron transfer cannot properly represent a system in which there are a very large number of quanta (as for $j \geq 7$) and many different vibrational modes are implicated in the excited-state distortion. In fact, eqs 31 and 32 give the most weight to the highest frequency vibrational modes (e.g., N−H or C−H) for which the values of j are relatively small. The vibrational reorganizational energies of these modes are very small (<30 cm^{-1}) as are the corresponding values of S_{MH} (<0.01), but the vibrational frequencies are very large so j can be in the range of 4−6 suggesting relatively large contributions; however, the kinetic effects of N−H or C−H perdeuteration are small and the contributions of these vibrational modes to the relaxation process must be very small.[26,81] The relatively good fit of 77 K decay rate constants for the $[Ru(Am)_{6-2n}(bpy)_n]^{2+}$ complexes to these equations by using values of $\Lambda_{x(max)}$ and $h\nu_{x(max)}$ obtained in the glassy matrices, as shown in Figure 9, is surprising.

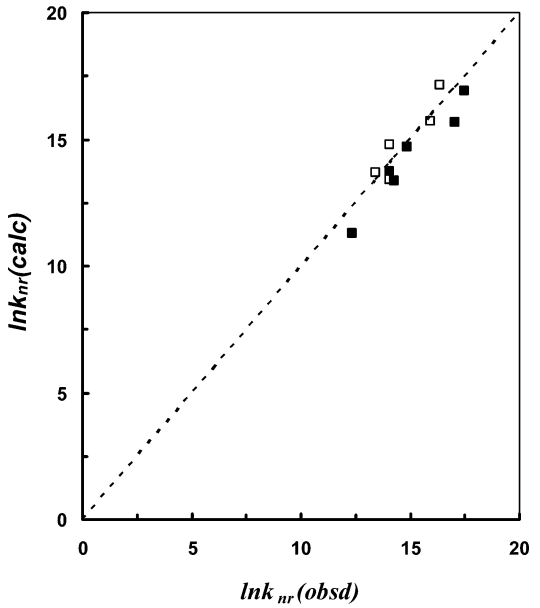

Figure 9. Correlation of nonradiative rate constant calculated from eq 32, $A = (3 \pm 2) \times 10^{13}$ s^{-1}, with that observed for $[Ru(Am)_{6-2n}(bpy)_n]^{2+}$ complexes in DMSO/water. Filled squares for am(m)ine (NH) complexes in DMSO/H_2O; open squares for deuterated am(m)ine (ND) complexes in DMSO/D_2O. Values of k_{nr}(obsd) from Table 1. The dashed line is drawn with a slope of 1.00. The sequence of complexes from top to bottom is the reverse of that in Figure 8.

Conclusions

We have found that the bipyridine ring vibrational reorganizational energy contributions to the 77 K emission spectra of $[Ru(Am)_{6-2n}(bpy)_n]^{2+}$ complexes are very strongly attenuated as the MLCT excited-state energy decreases. Reorganizational energy profiles (emreps) have been employed to demonstrate that these vibrational reorganizational energy contributions to the emission spectrum of $[Ru(NH_3)_4bpy]^{2+}$ are about half as large as those in the $[Ru(bpy)_3]^{2+}$ emission spectrum; thus, we find that the changes in either Λ_x or Λ_{1st} are proportional to the average changes in the vibrational reorganizational energies, $(\lambda_i)_{ave}$. This attenuation implies decreasing excited-state distortion concomitant with increasing electronic delocalization in the MLCT excited state ($\alpha_{eg}^2 \sim 0.1-0.3$) as bipyridine is replaced by am(m)ines through the series of complexes. The detailed analysis of the reorganizational energy attenuation is based on

modeling with previously reported resonance-Raman parameters. The published rR parameters fit the emission spectrum of $[Ru(NH_3)_4bpy]^{2+}$ very well. The fits of the $[Ru(bpy)_3]^{2+}$ emission spectrum are reasonable, but not as good, probably because the Franck−Condon excited state generated by absorption and probed by the rR is different in symmetry from the emitting MLCT excited state. Among the important inferences from the vibronic analysis are the following: (1) The dominant bpy-centered vibronic contribution to the emission spectrum is about half as large for $[Ru(NH_3)_4bpy]^{2+}$ as for $[Ru(bpy)_3]^{2+}$, but the absorption and emission maxima of $[Ru(NH_3)_4bpy]^{2+}$ span nearly the same energy range and the vibronic contributions to the emission are about 85% of those to the absorption (in DMSO/water; $I_{f(max)}$ adjusted to fit rR parameters); this is consistent with a spin constraint on the configurational mixing, which can be represented as $\alpha_{ge} > \alpha_{eg}$. (2) The attenuation is very large for $[Ru(NH_3)_4bpy]^{2+}$ with $\alpha_{eff}^2 \cong 0.35$ for the apparent squared mixing coefficient, and higher order correction terms must be important so that $\alpha_{eff}^2 < [\alpha_{ge}^2 + \alpha_{eg}^2]$. (3) Most of the amplitudes of the "vibronic sidebands" in 77 K emission spectra (and the skewness of ambient spectra) arise from the bandwidth contributions of overlapping vibronic contributions and not directly from the vibrational reorganizational energy contributions of high-frequency vibrational modes.

This rR-based modeling and the vibronic analysis of the emission spectra have illustrated some more general issues and raised others. It is clear that single high-frequency vibrational mode models do not adequately describe the 77 K emission spectra of these complexes. Thus, the modeling demonstrates that second- and third-order vibronic contributions must be included in order to account for the intensity and broadening on the low-energy side of the emission and that the apparent reorganizational energy (and, therefore, the apparent magnitude of the Huang−Rhys parameter, S_h) of any assumed single high-frequency mode is mostly a consequence of the overlapping contributions of many components with substantial bandwidths. The resonance-Raman data and the analysis presented in this paper indicate that the MLCT excited-state distortions involve small displacements in a large number of vibrational modes. This raises the possibility that the observed rate constants for nonradiative excited-state relaxation are the result of the sum contributions from a very large number of relaxation channels, each with a very small probability. Despite this demonstration that single high-frequency vibrational mode models incorrectly evaluate the excited-state distortion, such models can apparently provide good correlations of nonradiative rate constants under limited sets of conditions. This may arise from a weighted averaging of the very large number of most probable relaxation channels that approximates the overlapping vibronic contributions to the maxima of the difference spectra or of the emreps, but the origin and physical significance of such correlations are not clear at this time.

It seems likely that the spectral analysis employing emreps will prove useful in evaluating the variations in excited-state distortions for a series of related compounds even in the absence of additional information such as resonance-Raman data. Some limited extensions of this sort have been employed in the present report. We are currently exploring the extension of these approaches to a more diverse collections of compounds.

Appendix A: The Simulation of the Effects of Bandwidth Variations on the Emission Spectra and Emreps, Using a Resonance-Raman-Based Gaussian Band Model

1. The Overall Spectral Fittings. These are described in the text. We note that our procedure in effect normalizes the fitted intensity to the observed emission intensity and for convenience the intensity of the observed emission maximum is set equal to one. We have used the rR-based modeling to examine how the variations in bandwidth affect the evaluation of parameters in our spectral analysis.

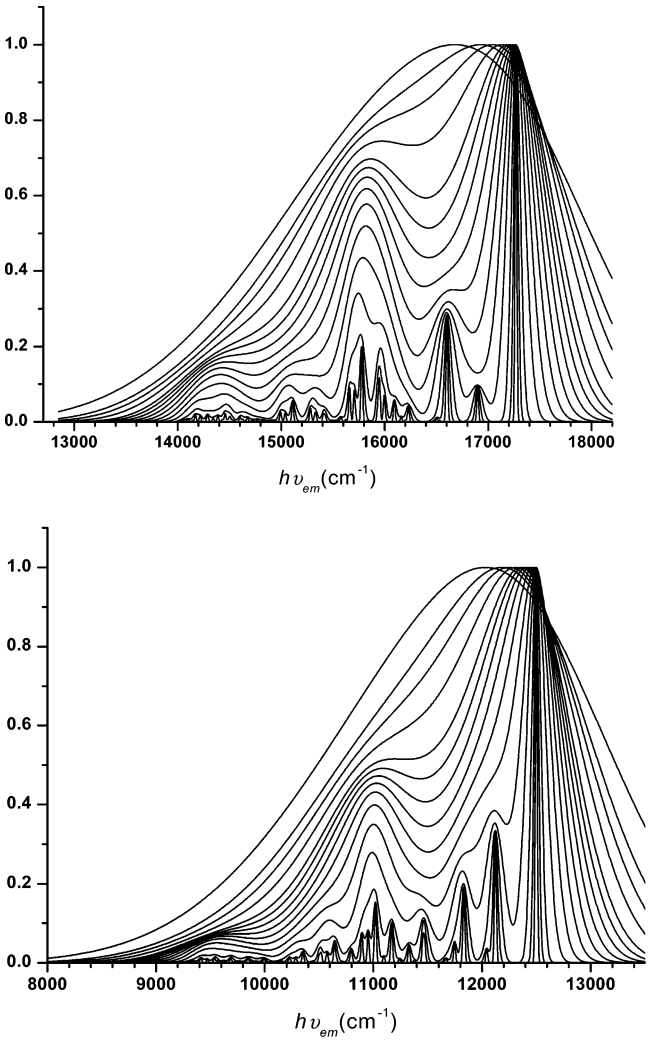

Figure 10. Effect of component bandwidth on emission spectra based on resonance-Raman modeling. Top, $[Ru(bpy)_3]^{2+}$, $h\nu_f = 17270$ cm^{-1} and component vibrational intensities adjusted to be 30% larger than those of $[Ru(NH_3)_4bpy]^{2+}$; bottom $[Ru(NH_3)_4bpy]^{2+}$, $h\nu_f = 12500$ cm^{-1}. Raman data from Table 2. Bandwidths, increasing from the bottom to top on the left-hand side of each figure: 20, 50, 100, 200, 300, 400, 500, 600, 700, 800, 900, 1100, 1300, 1500, and 2000 cm^{-1}.

2. The Variations in the Contributions of the Fundamental and the First-, Second-, and Third-Order Vibronic Components with Variations in Bandwidth. The overall effects of bandwidth on the emission spectra, based on the rR modeling, are shown in Figure 10.

a. The Effects of Component Bandwidth on the Evaluation of the Energy, Intensity, and Bandwidth of the Deconvoluted Fundamental. We have used eqs 9−13 and the rR data to calculate emission spectra for a range of bandwidths for $[Ru(bpy)_3]^{2+}$ and $[Ru(NH_3)_4bpy]^{2+}$. These calculated spectra were then deconvoluted using Grams32 and our usual procedures in order to simulate how variations in bandwidth will affect our evaluation of $I_{\nu_{m(f)}}$ from the experimental emission spectra. The dependence of the values of energy and intensity of the fundamentals from the deconvolution of the calculated spectra for $[Ru(bpy)_3]^{2+}$ and $[Ru(NH_3)_4bpy]^{2+}$ are shown in Figure 11. Since variations of $I_{\nu_{m(f)}}$with $\Delta\nu_{1/2}$ can seriously affect the

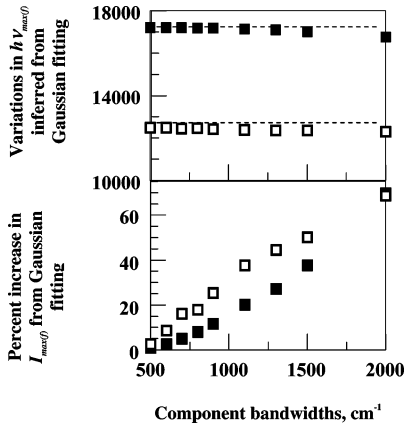

Figure 11. The variations with component bandwidth (top) and the intensity (bottom) of the fundamental component obtained from the Gaussian (Grams32) deconvolution of spectra calculated from the resonance-Raman parameters of $[Ru(bpy)_3]^{2+}$ (filled squares) adjusted so that the intensities of the vibronic components were 1.5 times those of the $[Ru(NH_3)_4bpy]^{2+}$ (open squares) vibronic components. The input intensities of the fundamental components were set equal to one for the calculated spectra. The horizontal dashed lines in the top figure are drawn as aids in evaluating the deviations.

evaluation of the changes in reorganizational energy through a series of complexes, we have used Figure 11 as a basis for correcting for these effects.

b. The Effects of Component Bandwidth on the Evaluation of the Energy, Intensity, and Bandwidth of the Fundamental Fitted to the rR Data. The bandwidths of the fundamentals fitted to the rR data vary linearly with the input bandwidths (over the same range as above); the fits are given by eqs 21 and 22.

c. Effects of Component Bandwidth on Difference Spectrum Band Shapes and Intensities: *Contributions of the First-, Second-, and Third-Order Vibronic Components Based on rR Parameters.* The band shapes are very strongly dependent on the bandwidth as shown in Figure 10. The intensities calculated by eqs 11−15 are the integrated intensities, proportional to the contributing oscillator strengths of the emission components. For a given set of conditions, the integrated intensity, I_h, of a component is expected to be a constant; the intensity of the maximum for a Gaussian component h (and a constant $c \cong 1.05$)[4] is given by,

$$I_{\max(h)} = I_h/(c\Delta\nu_{1/2}) \qquad \text{(A1)}$$

Since we do not determine the total intensity, or emission yield, and since we adjust the maximum of the emission spectra to unity before deconvoluting, eq A1 is not directly applicable to our analysis of the spectra. Since the component reorganizational energies are proportional to the ratio of an observed intensity to the intensity of the fundamental (eq 2), they are not functions of the absolute intensity (or quantum yield) and they are relatively weakly dependent on bandwidth. The Grams32 deconvolutions give us values of $I_{\max(f)}$ that are larger than those obtained after adjustment for the contributions of rR vibronic components largely because the vibronic components with $h\nu_h < \sim \Delta\nu_{1/2}$ are partly or completely convoluted into the estimate of the fundamental obtained from the Grams32 procedure. The use of the fundamental so obtained results in a very poor fit of the difference spectrum in the low-frequency region ($\Delta\nu_d <$ 500 cm^{-1}); compare Figures 5 and 12. There is some dependence of the emreps on bandwidth and this dependence is discussed below. An important contribution to the band shape and to the relative intensity of the vibronic contributions arises

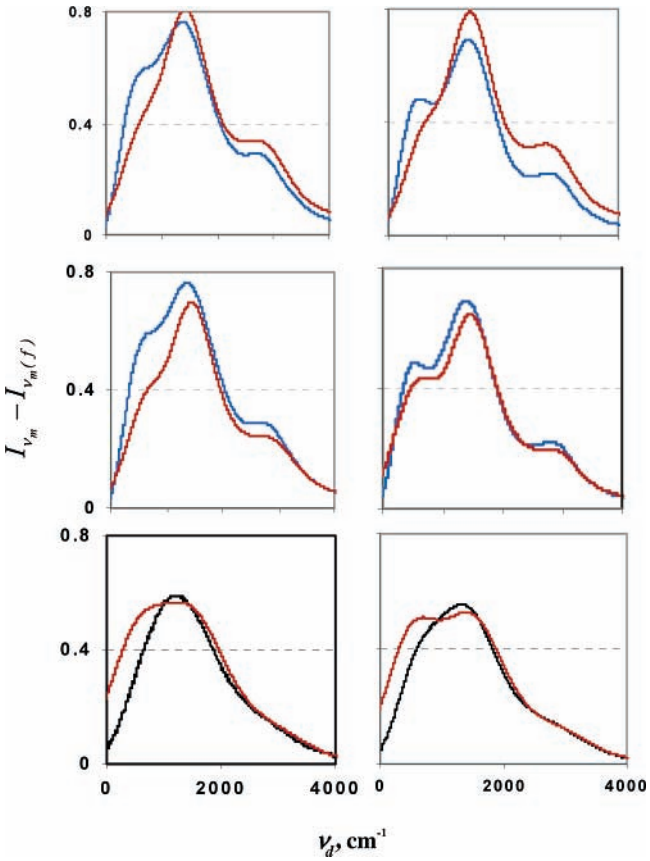

Figure 12. Difference spectra obtained by subtracting the fundamental inferred from Grams32 fits from the experimental emission spectra, black curves, and the difference spectra based on the fits of the resonance-Raman parameters, red curves. For 77 K emission spectra obtained in DMSO/water, left column, and butyronitrile, right column; $[Ru(bpy)_3]^{2+}$ with the calculated difference spectrum based on the reported rR parameters, top row; $[Ru(bpy)_3]^{2+}$ with the calculated difference spectrum based on the rR reorganizational parameters adjusted to 1.4 times the corresponding reorganizational energies of $[Ru(NH_3)_4bpy]^{2+}$, middle left; $[Ru(bpy)_3]^{2+}$ with the calculated difference spectrum based on rR reorganizational parameters adjusted to 1.3 times the corresponding reorganizational energies of $[Ru(NH_3)_4bpy]^{2+}$, middle right; $[Ru(NH_3)_4bpy]^{2+}$, bottom row. $I_{\max(f)} = 1$ for these fittings.

when several vibronic components are close enough in energy that their associated intensity distributions overlap; this is illustrated in Figure 10. The net intensity at a specific frequency can also increase due to the increasing percentage contributions of second and higher order contributions; see Figure 13. The effects of bandwidth on the contributions of the first- and second-order vibronic contributions to intensity near to 1500 cm^{-1} are summarized in Table 5.

3. The Evaluation of Emrep Properties Based on rR Models. Since the emreps are obtained as a ratio of the intensity observed to that of the fundamental, the emreps are more weakly dependent on bandwidth than are the difference spectra. Even so, Figure 14 suggests that most (approximately 60−80% at 77 K and a much larger percentage at 300 K) of the amplitudes of the emreps result from the substantial component bandwidths when many vibrational modes contribute to the excited-state distortion. The component reorganizational energies are recovered in emreps when the bandwidths become sufficiently small; see Figure 14. If the excited-state distortion were correlated to a single vibronic mode, then the amplitude of the emrep would correspond to the reorganizational energy of that mode. It is clear that the representation of a multimode distortion by a single vibrational mode results in a very large overestimate of the

TABLE 5: The Resonance-Raman Modeled Contributions of First- and Second-Order Vibronic Components to the Emission Spectrum of (a) $[Ru(NH_3)_4bpy]^{2+}$ at $h\nu_{x(max)} = 1481\ cm^{-1}$ and (b) $[Ru(bpy)_3]^{2+}$ at $h\nu_{x(max)} = 1493\ cm^{-1}$

(a) $[Ru(NH_3)_4bpy]^{2+}$

assumed $\Delta\nu_{1/2}$, cm^{-1}	total intensity $I_{1481(T)}$	$I_{1481(0'1)}$	$I_{1481(0'2)}$	$I_{1481(0'0)}$	$I_{1481(0'1)}/I_{1481(T)}$	$I_{1481(0'2)}/I_{1481(T)}$
500	0.46782	0.36677	0.10106	2.73E−11	0.784	0.21602
600	0.52122	0.38964	0.13158	4.62E−08	0.74755	0.25245
700	0.57259	0.41027	0.16231	4.08E−06	0.71652	0.28347
800	0.62317	0.43137	0.19173	7.48E−05	0.69222	0.30767
900	0.67412	0.45457	0.219	5.49E−04	0.67432	0.32487
1100	0.78135	0.50847	0.26632	0.00657	0.65076	0.34085
1300	0.90028	0.56795	0.30495	0.02738	0.63086	0.33873
1500	1.03022	0.62643	0.33676	0.06703	0.60805	0.32688
2000	1.36112	0.74718	0.39526	0.21867	0.54894	0.29039

(b) $[Ru(bpy)_3]^{2+}$

assumed $\Delta\nu_{1/2}$, cm^{-1}	total intensity $I_{1493(T)}$	$I_{1493(0'1)}$	$I_{1481(0'2)}$	$I_{1493(0'0)}$	$I_{1493(0'1)}/I_{1493(T)}$	$I_{1493(0'2)}/I_{1493(T)}$
500	0.65646	0.57597	0.08049	1.85E−11	0.87739	0.12261
600	0.71801	0.61399	0.10402	3.52E−08	0.85513	0.14487
700	0.77364	0.64516	0.12848	3.34E−06	0.83393	0.16607
800	0.82693	0.67399	0.15287	6.42E−05	0.81505	0.18486
900	0.87951	0.70247	0.17656	4.87E−04	0.79871	0.20075
1100	0.98613	0.75899	0.22108	0.00606	0.76967	0.22419
1300	1.1	0.81196	0.26219	0.02585	0.73815	0.23835
1500	1.22315	0.85853	0.30042	0.0642	0.7019	0.24561

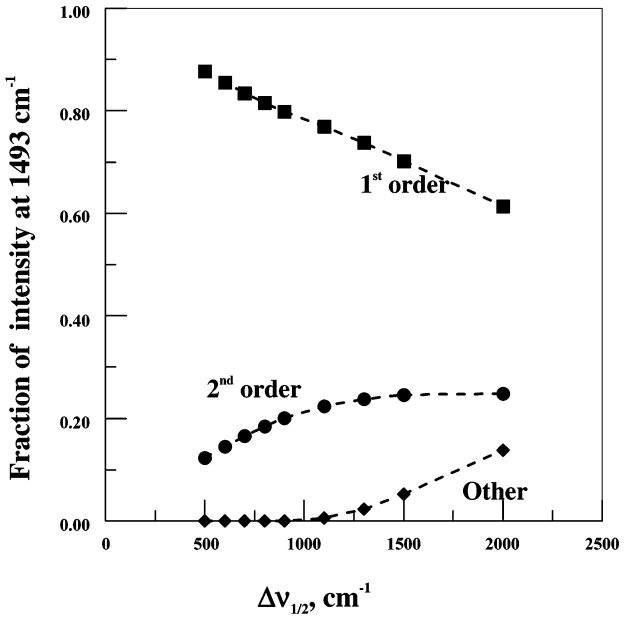

Figure 13. Variations of the amplitudes at 1493 cm^{-1} of the first-order vibronic contributions (squares) and second-order vibronic contributions (circles) to the spectra calculated for $[Ru(bpy)_3]^{2+}$. The contributions of the fundamental plus the third-order vibronic contributions are indicated by the diamonds. Based on rR parameters for $[Ru(bpy)_3]^{2+}$ with vibrational reorganizational energies adjusted to be 50% larger than those of $[Ru(NH_3)_4bpy]^{2+}$.

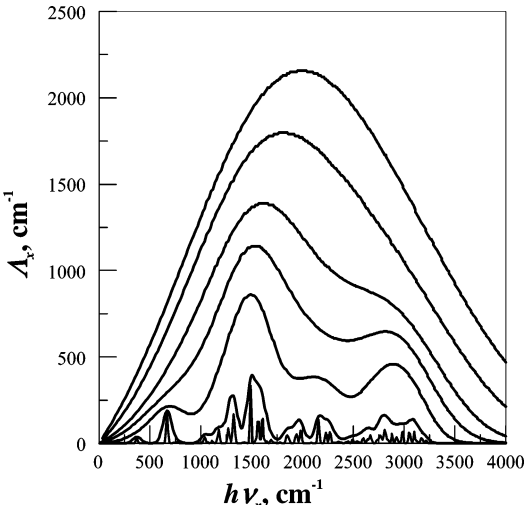

Figure 14. The dependence of the emreps for $[Ru(bpy)_3]^{2+}$ on component bandwidths. The reorganizational energies of the resonance-Raman frequencies are 1.5 times the reorganizational energies of the comparable frequencies for $[Ru(NH_3)_4bpy]^{2+}$. The bandwidths are, from bottom to top: 20, 100, 400, 700, 1000, 1500, and 2000 cm^{-1}.

reorganizational energy associated with the distortion; it would also result in an incorrect evaluation of the molecular structure of the excited state. The modeling with rR parameters suggests that the correction of emreps to a common bandwidth through the series of complexes for $[Ru(bpy)_3]^{2+}$ is given by

$$\Lambda_{x(corr)} = \Lambda_{x(max)}(1 - (3.27 \pm 0.09)|\partial\Delta\nu_{1/2}| \times 10^{-4}) \quad \text{(A2)}$$

For $[Ru(NH_3)_4bpy]^{2+}$,

$$\Lambda_{x(corr)} = \Lambda_{x(max)}(1 - (4.89 \pm 0.17)|\partial\Delta\nu_{1/2}| \times 10^{-4}) \quad \text{(A3)}$$

And interpolated for $[Ru(NH_3)_2(bpy)_2]^{2+}$,

$$\Lambda_{x(corr)} = \Lambda_{x(max)} \times (1 - (4.04 \pm 0.13)|\partial\Delta\nu_{1/2}| \times 10^{-4}) \quad \text{(A4)}$$

Since the rR data give good simulations of the emission spectra of $[Ru(bpy)_3]^{2+}$ and $[Ru(NH_3)_4(bpy)]^{2+}$, they can be used to evaluate and/or model aspects of the emreps in the region of the bpy vibrational modes. This use of the rR data to model the emission spectra enables us to start with a set of known reorganizational (or displacement) parameters and inquire how the information about excited-state structure is altered by the variations in bandwidth, and how much information can be extracted from the spectral analyses described herein. The issues of greatest concern to us are:(1) to what extent can the vibronic envelope of an emission spectrum, evaluated as either a difference spectrum or as an emrep, provide useful information

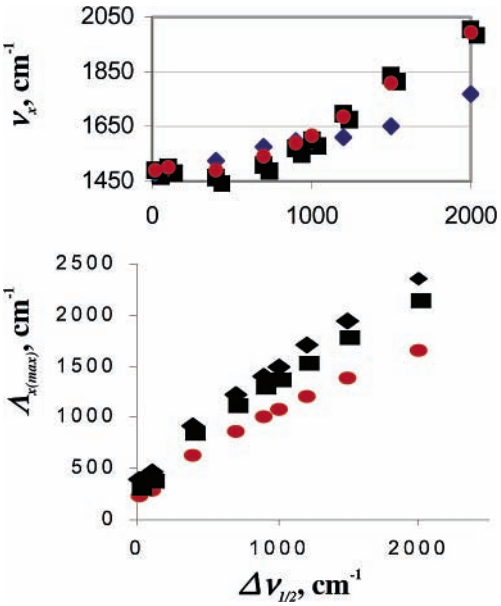

Figure 15. Resonance-Raman-based modeling of the bandwidth dependence of emrep parameters: $\nu_{x(max)}$, top, and $\Lambda_{x(max)}$, bottom. For $[Ru(NH_3)_4bpy]^{2+}$, red; original rR intensities for $[Ru(bpy)_3]^{2+}$, black diamonds; $[Ru(bpy)_3]^{2+}$ adjusted to 1.5 times those of $[Ru(NH_3)_4bpy]^{2+}$, black squares.

about the excited-state distortion (i.e., about the actual contributions of the displacement modes) and (2) how quantitatively can the differences in these vibronic envelopes be used to probe differences in excited-state distortions in a related series of complexes?

The experimental and calculated emreps are compared in Figure 6. The calculated reorganizational energies are reasonably consistent with those obtained from the experimental (77 K) spectra: the energy and amplitude of the major vibronic contributions at about 1500 cm^{-1} are reproduced reasonably well (these, largely first-order component contributions are reproduced very well for the rR parameters of $[Ru(bpy)_3]^{2+}$ adjusted to be 1.5 times those of $[Ru(NH_3)_4bpy]^{2+}$). The ratios of emreps of different compounds are only weakly dependent on the bandwidth (see Figure 3) and this suggests that useful information about the differences in multimode excited-state distortions of a series of complexes can be obtained, with relatively small corrections, from the emreps of complexes with substantial component bandwidths.

Acknowledgment. The authors thank the Office of Basic Energy Sciences of the Department of Energy for partial support of this research.

Supporting Information Available: Synthetic details, details of the procedures for generating emreps, tables of parameters, and tables of data. This material is available free of charge via the Internet at http://pubs.acs.org.

References and Notes

(1) Shin, Y. K.; Brunschwig, B. S.; Creutz, C.; Sutin, N. *J. Phys. Chem.* **1996**, *100*, 8157.
(2) Brunschwig, B. S.; Creutz, C.; Sutin, N. *Coord. Chem. Rev.* **1998**, *177*, 61.
(3) Seneviratne, D. S.; Uddin, M. J.; Swayambunathan, V.; Schlegel, H. B.; Endicott, J. F. *Inorg. Chem.* **2002**, *41*, 1502.
(4) Mulliken, R. S.; Person, W. B. *Molecular Complexes*; Wiley-Interscience: New York, 1967.
(5) Hush, N. S. *Electrochim. Acta* **1968**, *13*, 1005.
(6) Hush, N. S. *Prog. Inorg. Chem.* **1968**, *8*, 391.
(7) Marcus, R. A. *J. Phys. Chem.* **1990**, *94*, 4963.
(8) Matyushov, D. V.; Voth, G. A. *J. Phys. Chem. A* **2000**, *104*, 6470.
(9) Matyushov, D. V.; Newton, M. D. *J. Phys. Chem. A* **2001**, *105*, 8516.
(10) Solomon, E. I. *Comments Inorg. Chem.* **1984**, *3*, 227.
(11) Brunold, T. C.; Gudel, H. U. In *Inorganic Electronic Structure and Spectroscopy*; Solomon, E. I., Lever, A. B. P., Eds.; Wiley-Interscience: New York, 1999; Vol. 1, p 259.
(12) Gould, I. R.; Noukakis, D.; Luis, G.-J.; Young, R. H.; Goodman, J. L.; Farid, S. *Chem. Phys.* **1993**, *176*, 439.
(13) Graff, D.; Claude, J. P.; Meyer, T. J. In *Electron Transfer in Organometallic and Biochemistry*; Isied, S. S., Ed.; American Chemical Society: Washington, DC, 1997; p 183.
(14) Endicott, J. F. In *Comprehensive Coordination Chemistry II*; McCleverty, J., Meyer, T. J., Eds.; Pergamon: Oxford, UK, 2003; Vol. 7; p 657.
(15) Marcus, R. A. *J. Phys. Chem.* **1989**, *93*, 3078.
(16) Endicott, J. F.; Chen, Y.-J.; Xie, P. *Coord. Chem. Rev.* **2005**, *249*, 343.
(17) Xie, P.; Chen, Y.-J.; Endicott, J. F.; Uddin, M. J.; Senerivatne, D.; McNamara, P. G. *Inorg. Chem.* **2003**, *42*, 5040.
(18) Hupp, J. T.; Williams, R. T. *Acc. Chem. Res.* **2001**, *34*, 808.
(19) Maruszewski, K.; Bajdor, K.; Strommen, D. P.; Kincaid, J. R. *J. Phys. Chem.* **1995**, *99*, 6286.
(20) Crosby, G. A. *Acc. Chem. Res.* **1975**, *8*, 231.
(21) Juris, A.; Barigelletti, F.; Compangna, S.; Balzani, V.; Belser, P.; von Zelwesky, A. *Coord. Chem. Rev.* **1988**, *84*, 85.
(22) Kalyanasundaram, K. *Photochemistry of Polypyridine and Porphyrin Complexes*; Academic Press: New York, 1992.
(23) Lever, A. B. P.; Dodsworth, E. In *Electronic Structure and Spectroscopy of Inorganic Compounds*; Lever, A. B. P., Solomon, E. I., Eds.; Wiley: New York, 1999; Vol. II, p 227.
(24) Meyer, T. J. *Progr. Inorg. Chem.* **1983**, *30*, 389.
(25) Barbara, P. F.; Meyer, T. J.; Ratner, M. *J. Phys. Chem.* **1996**, *100*, 13148.
(26) Van Houten, J.; Watts, R. J. *J. Am. Chem. Soc.* **1975**, *97*, 3843.
(27) Yersin, H.; Braun, D.; Hensler, G.; Galhuber, E. In *Vibronic Processes in Inorganic Chemistry*; Flint, C. D., Ed.; Kluwer: Dordrecht, The Netherlands, 1989; p 195.
(28) Balzani, V.; Juris, A.; Venturi, D.; Campagna, S.; Serroni, S. *Chem. Rev.* **1996**, *96*, 956.
(29) Krausz, E.; Ferguson, J. *Progr. Inorg. Chem.* **1989**, *37*, 293.
(30) Krausz, E. *Chem. Phys. Lett.* **1987**, *135*, 249.
(31) Yersin, H.; Braun, D. *Chem. Phys. Lett.* **1991**, *179*, 85.
(32) Yersin, H.; Humbs, W.; Strasser, J. *Coord. Chem. Rev.* **1997**, *159*, 325.
(33) Lever, A. B. P.; Gorelsky, S. I. *Coord. Chem. Rev.* **2000**, *208*, 153.
(34) Damarauer, N. H.; Cerullo, G.; Yeh, A.; Boussie, T. R.; Shank, C. V.; McCusker, J. K. *Science* **1997**, *275*, 54.
(35) Yeh, A. T.; Shank, C. V.; McCusker, J. K. *Science* **2000**, *289*, 935.
(36) McCusker, J. K. *Acc. Chem. Res.* **2003**, *36*, 876.
(37) Bhasikuttan, A. C.; Suzuki, M.; Nakashima, S.; Okada, T. *J. Am. Chem. Soc.* **2002**, *124*, 8398.
(38) Hannappel, T.; Bernd, B.; Storck, W.; Willig, F. *J. Phys. Chem. B* **1997**, *101*, 6799.
(39) Meier, A.; Selmarten, D. C.; Seiemoneit, K.; Smith, B. B.; Nozik, A. J. *J. Phys. Chem. B* **1999**, *103*, 2122.
(40) Birks, J. B. *Photophysics of Aromatic Molecules*; Wiley-Interscience: New York, 1970.
(41) Myers, A. B. *Chem. Phys.* **1994**, *180*, 215.
(42) Myers, A. B. In *Laser Techniques in Chemistry*; Myers, A. B., Rizzo, T. R., Eds.; John Wiley & Sons: New York, 1995; Vol. XXIII, p 325.
(43) Myers, A. B. *Chem. Rev.* **1996**, *96*, 911.
(44) Myers, A. B. *Acc. Chem. Res.* **1998**, *30*, 5519.
(45) Englman, R.; Jortner, J. *Mol. Phys.* **1970**, *18*, 145.
(46) Freed, K. F.; Jortner, J. *J. Chem. Phys.* **1970**, *52*, 6272.
(47) Hush, N. S. *Trans. Faraday Soc.* **1961**, *57*, 557.
(48) Marcus, R. A. *Discuss. Faraday Soc.* **1960**, *29*, 21.
(49) Marcus, R. A. *Annu. Rev. Phys. Chem.* **1964**, *15*, 155.
(50) Marcus, R. A. *J. Chem. Phys.* **1965**, *43*, 670.
(51) Cannon, R. D. *Adv. Inorg. Chem. Radiochem.* **1979**, *21*, 179.
(52) Endicott, J. F.; Brubaker, G. R.; Ramasami, T.; Kumar, K.; Dwarakanath, K.; Cassel, J.; Johnson, D. *Inorg. Chem.* **1983**, *22*, 3754.
(53) Meyer, T. J.; Taube, H. In *Comprehensive Coordination Chemistry*; Wilkinson, G., Ed.; Pergamon: Oxford, England, 1987; Vol. 7, p 331.
(54) Newton, M. D.; Sutin, N. *Annu. Rev. Phys. Chem.* **1984**, *35*, 437.
(55) Richardson, D. E. In *Inorganic Electronic Structiure and Spectroscopy*; Solomon, E. I., Lever, A. B. P., Eds.; Wiley: New York, 1999; Vol. II, p 131.
(56) Sutin, N. *Acc. Chem. Res.* **1982**, *15*, 275.
(57) Sutin, N. *Progr. Inorg. Chem.* **1983**, *30*, 441.
(58) Sutin, N. *Adv. Chem. Phys.* **1999**, *106*, 7.

(59) Endicott, J. F.; Schegel, H. B.; Uddin, M. J.; Senerivatne, D. *Coord. Chem. Rev.* **2002**, *229*, 95.
(60) Endicott, J. F.; Uddin, M. J.; Schlegel, H. B. *Res. Chem. Intermed.* **2002**, *28*, 761.
(61) Creutz, C.; Newton, M. D.; Sutin, N. *Photochem. Photobiol. A*: *Chem.* **1994**, *82*, 47.
(62) Hush, N. S. In *Mechanistic Aspects of Inorganic Reactions*; Rorabacher, D. B., Endicott, J. F., Eds.; ACS Symp. Ser. 198; American Chemical Society: Washington, DC, 1982; p 301.
(63) Matyushov, D. V.; Voth, G. A. In *Reviews in Computational Chemistry*; Lipkowitz, K. B., Boyd, D. B., Eds.; Wiley-VCH: New York, 2002; Vol. 18, p 147.
(64) Chen, Y.-J.; Xie, P.; Endicott, J. F. *J. Phys. Chem. A* **2004**, *108*, 5041.
(65) Dixon, N. E.; Lawrence, A.; Lay, P. A.; Sargeson, A. M.; Taube, H. *Inorg. Synth.* **1986**, *24*, 243.
(66) Callahan, R. W.; Brown, G. M.; Meyer, T. J. *Inorg. Chem.* **1975**, *14*, 1443.
(67) Brown, G. M.; Sutin, N. *J. Am. Chem. Soc.* **1979**, *101*, 883.
(68) Brown, G. M.; Kreutzian, H. J.; Abe, M.; Taube, H. *Inorg. Chem.* **1979**, *18*, 3374.
(69) Krause, R. A. *Inorg. Chim. Acta* **1977**, *209*, 213.
(70) Bryant, G. M.; Ferguson, J. E.; Powell, H. K. *Austr. J. Chem.* **1971**, *24*, 257.
(71) Sakai, K.; Yamada, Y.; Tsubomura, T. *Inorg. Chem.* **1996**, *35*, 3163.
(72) Supporting Information available, see paragraph at the end of the paper.
(73) Endicott, J. F. In *Electron Transfer in Chemistry*; Balzani, V., Ed.; Wiley-VCH: New York, 2001; Vol. 1, p 238.
(74) Yardley, J. T. *Introduction to Molecular Energy Transfer*; Academic: New York, 1980.
(75) Gorelsky, S. I.; Kotov, V. Y.; Lever, A. B. P. *Inorg. Chem.* **1998**, *37*, 4584.
(76) Thompson, D. G.; Schoonover, J. R.; Timpson, C. J.; Meyer, T. J. *J. Phys. Chem. A* **2003**, *107*, 10250.
(77) Lever, A. B. P. *Inorganic Electronic Spectroscopy*; Elsevier: Amsterdam, The Netherlands, 1984.
(78) Chen, J. Y.; Xie, P.; Endicott, J. F. Manuscript in preparation.
(79) Song, X.; Endicott, J. F. *Chem. Phys. Lett.* **1993**, *204*, 400.
(80) Boraselli, C. D.; Bratalovsky, S. E. *J. Phys. Chem.* **1998**, *102*, 6231.
(81) Chen, Y.-J.; Xie, P.; Endicott, J. F. Work in progress.